QUANTIFICATION AND CHARACTERIZATION OF PARTICULATE MATTER IN POLYURETHANE SHAPE MEMORY FOAMS AND FOAM-BASED DEVICES

A Thesis

by

ADAM LLOYD NATHAN

Submitted to the Office of Graduate and Professional Studies of
Texas A&M University
in partial fulfillment of the requirements for the degree of

MASTER OF SCIENCE

Chair of Committee,	Duncan J. Maitland
Committee Members,	Balakrishna Haridas
	Wayne Hung
Head of Department	Anthony Guiseppi-Elie

May 2016

Major Subject: Biomedical Engineering

ABSTRACT

Endovascular therapy involves the placement of an implantable filler coil directly into an aneurysm sac to occlude the space and promote healing of the damaged vessel wall. Implantable devices must be tested to assess and address all potential risks that they may pose. Shape memory polymer (SMP) foams have been placed over nitinol coils as an endovascular treatment option for cerebral aneurysms. These foams have large potential for use in aneurysm embolization, but it is unknown whether they will generate harmful particulate matter upon implantation into the body. Particulates could be the result of damaged or weakened foam struts that are prone to fracture upon agitation or external forces. Currently, there are no existing protocols for the quantification of particulate matter in SMP embolic devices. The focus of this work was to investigate particulate levels in SMP foams and foam devices.

Protocols were developed to quantify particulate formation in a foam cleaning process, two reticulation processes, and device delivery. Furthermore, visual characterization and cytocompatibility testing was performed on SMP foam particulates. Results from the studies demonstrated that the foams and foam-based devices generate particulate levels that are in compliance with limits stated by the most relevant standard. When concentrated particulate treatments were administered to fibroblasts, they exhibited high cell viability (100%). These results provide further validation of the use of SMP materials in a neurovascular embolization device.

DEDICATION

To my parents, my mother who was the first to push me to do better and try harder. She was the person who sparked my love for science and math, and she helped me to recognize my true potential as an engineer. My father showed me what it means to truly work hard. With enough sweat and commitment, anything can get done. Both of my parents have sacrificed so much for me to get here and I just want to express my gratitude. Whenever times got tough, I used your sacrifice to help press onward and keep working.

Morgan, since the day we met, you have been supportive of every endeavor that I took part in. Regardless of how much dislike you had for what I was doing, you were selfless in your love and support of it. You kept me focused during all of my late nights studying and writing, and you were there to force me to take a break and destress. You were my home away from home, and for that, I thank you.

ACKNOWLEDGEMENTS

I want to thank my committee chair, Dr. Duncan Maitland for his guidance and support of my growth as a researcher. Regarding research, I entered Texas A&M as an unshapen lump of clay, and Dr. Maitland helped shape me into what I believe is a pretty good researcher. He was patient with my mistakes and steered me back onto the right course when I was drifting astray. Under his mentorship, I feel that I got more than just a Master's of Science degree during my two years here at A&M. The Biomedical Device Lab (BDL) has helped me bridge the gap between being a good student to being a good employee in the medical industry. I couldn't imagine a better place to perform my graduate studies than at the BDL under Dr. Maitland's guidance. Dr. Maitland's lab was once described to me as "being thrown into the deep end when learning to swim. But as you're thrashing around thinking you're drowning, you look down and realize that Dr. Maitland gave you two little floaties on your arms and that everything's going to be okay." It was a heck of a way to learn to swim, but I wouldn't have had it any other way. Thank you Dr. Maitland.

I want to thank Dr. Haridas and Dr. Hung for their guidance throughout the completion of my thesis. Both of you were eager to hear about my developments and you provided me with much needed insight into the intricacies of my experiments and research problems. You were always willing to take time out of your busy schedules to meet with me or sign a form, or look over some data, and I am grateful.

I would also like to thank Dr. Mary Beth Monroe for her help in compiling manuscripts, editing, and research advice. You always seem to find time to be able to meet or respond to

my late night emails. I am extremely grateful for all the time and effort that you have put forth towards helping me become a better writer.

I want to thank Dr. Wonjun Hwang for your patience and mentorship during my early months as an engineer. You really set the standard for my research and provided a foundation for the thought processes behind solving research problems. Thank you for your help developing the particulate protocols and troubleshooting the experimental setup.

I cannot begin to put words to how much my peers in the BDL meant to me during my time at Texas A&M. They offered support, guidance, criticism, and distraction from my research. I was honored to work alongside such exceptional engineers. They pushed me to be better and work harder day in and day out. Coming into the office every day was truly a joy and I will never forget you guys.

Lastly, I would like to than Dr. Martinez from Westminster Christian High School. Your passion and love for the sciences was what motivated me to pursue a degree in biomedical engineering. I can't thank you enough for what you've taught me, and I will be forever grateful for the lessons that I learned from you.

NOMENCLATURE

AAMI	Association for Advancement of Medical Instrumentation
Al_2O_3	Aluminum oxide
$CaCl_2$	Calcium chloride
CF_4	Tetrafluoromethane
DI	Deionized
DMEM	Dulbecco's modified eagle medium
FDA	Food and Drug Administration
FOC	Foam-over-coil
HDI	hexamethylene diisocyanate
HPED	N,N,N',N'-tetrakis(2-hydroxypropyl) ethylenediamine
IPA	Isopropyl alcohol
LO	Light obscuration
MRA	Magnetic Resonance Angiography
MTS	Insight Material Tester
NBCS	Newborn calf serum
NED	Neurovascular embolization device
NR	Neutral red
O_2	Oxygen
OD_{540}	Optical density at 540 nm
OH	Hydroxyl
P/S	Penicillin/streptomycin

RO	Reverse osmosis
SAH	Subarachnoid hemorrhage
SD	Standard deviation
SEM	Scanning electron microscopy
SMP	Shape memory polymer
SiO_2	Silicon dioxide
TEA	triethanolamine
T_g	Glass transition temperature
TIR	Technical information report
T_m	Melt transition temperature
TMHDI	trimethyl-1,6-hexamethylene diisocyanate
T_{trans}	Transition temperature
USP	United States Pharmacopeia
UV	Ultraviolet
Vol%	Volume percentage
W	Tungsten
Wt%	Weight percentage

TABLE OF CONTENTS

Page

LIST OF FIGURES

LIST OF TABLES

CHAPTER I

INTRODUCTION

1.1. Shape memory polymer (SMP) foam

SMPs are "smart" materials capable of maintaining a secondary geometry and then returning to a primary geometry upon application of a thermal, chemical, or optical stimulus (**Figure 1.1**)[1,2]. The majority of SMPs exhibit thermally activated behavior[3]. Thermal SMPs form their primary shape at a temperature greater than their transition temperature (T_{trans}). That primary shape is fixed *via* cooling and/or cross-linking. The secondary shape is set *via* deformation of the polymer while it is in its rubbery state at a temperature above T_{trans}, and stabilized by cooling back to its glassy state below T_{trans}. Upon supplying thermal energy to the SMP (heat above T_{trans}), there is sufficient entropic potential to drive shape recovery to the primary shape[1]. SMPs networks are made up of net-points and switching segments; the net points determine the permanent shape, and the switching segments absorb stress and permit deformation once heated above T_{trans}[1]. SMPs that are predominantly crystalline have a T_{trans} equal to their melt transition temperature (T_m), and SMPs that are predominantly amorphous have a T_{trans} equal to their glass transition temperature (T_g)[1].

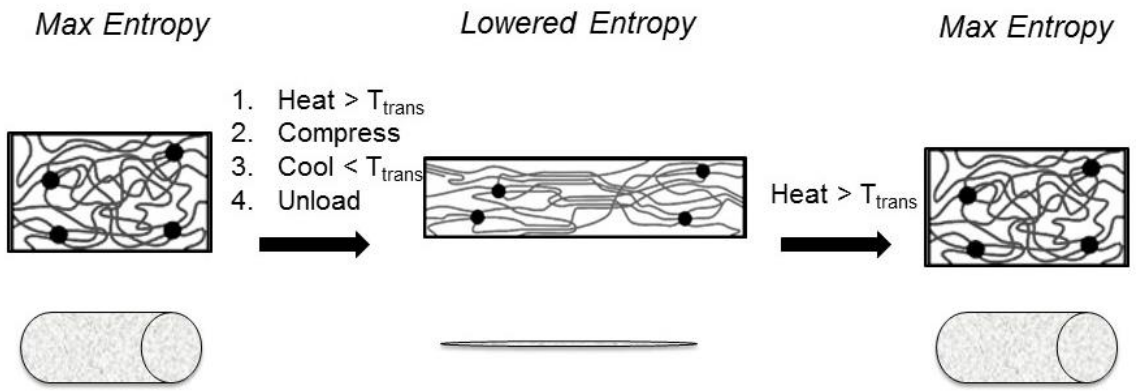

Figure 1.1: Mechanism by which a SMP foam is compressed into a secondary geometry and returned back to its primary geometry.

Specifically, the SMPs used here are polyurethane SMP foams. Polyurethane SMP foams exhibit a large T_g range (-100° C to +80° C), ultra-low densities, high porosity, X-ray visibility, capability for catheter delivery, low processing costs, and thermal stability[4-8]. The foams demonstrated exceptional biocompatibility, a reduced inflammatory response, the capability for interconnected thrombus formation, and aneurysm healing in an *in vivo* study in a porcine aneurysm model[9-11].

1.2. Neurovascular embolization for prevention of cranial aneurysms

SMP foams are being considered as embolization materials for a number of biomedical applications. Each application has its own set of requirements regarding foam porosity, optimal foam volume, actuation time, and mechanical properties. These SMP foams exhibit low densities, highly tunable thermal and mechanical properties[12,13], high volume recovery[14], easy processability[4], and exceptional biocompatibility[9,10] making them ideal candidates for neurovascular embolization devices (NEDs).

An aneurysm is a localized abnormal dilation of a blood vessel, resulting from a weakened or damaged vascular wall, often a side effect of atherosclerosed vascular tissue[15,16].

Aneurysms may be congenital or acquired and occur at damage sites on vessel walls[17]. Typical locations include the aorta, peripheral vasculature, and the mesenteric (intestinal), splenic, and cerebral arteries[18]. They can be fusiform, false, or saccular aneurysms[17]. This work focuses on cerebral saccular aneurysms, spherical outpouchings ranging from 2 to 50 mm in diameter (average diameter = 8 mm) involving only a portion of the vessel wall[17]. In a Japanese study magnetic resonance angiography (MRA) was performed on 8,500 healthy, asymptomatic individuals; 3.2% of patients contain at least one unruptured saccular aneurysm in the cranial region[19]. The majority of intracranial saccular aneurysms develop at the apex of the subarachnoid arterial bifurcations[20]. If an aneurysm bursts, it results in subarachnoid hemorrhage (SAH), which affects as many as 30,000 Americans each year[15,16]. SAH causes a reduction in cerebral blood flow coupled with reduced cerebral autoregulation that leads to acute ischemia or stroke. Stroke causes an increase in intracranial blood pressure, decreased blood perfusion and acute vasoconstriction[16], all of which pose a significant risk of decreasing the patient's mental health, permanently damaging the brain, or even death. Patient mortality following SAH is as high as 50%, and there is substantial morbidity among survivors[16]. Currently, the primary treatment modalities for aneurysms to prevent SAH are surgical clipping and filling with endovascular coils (**Figure 1.2A-B**).

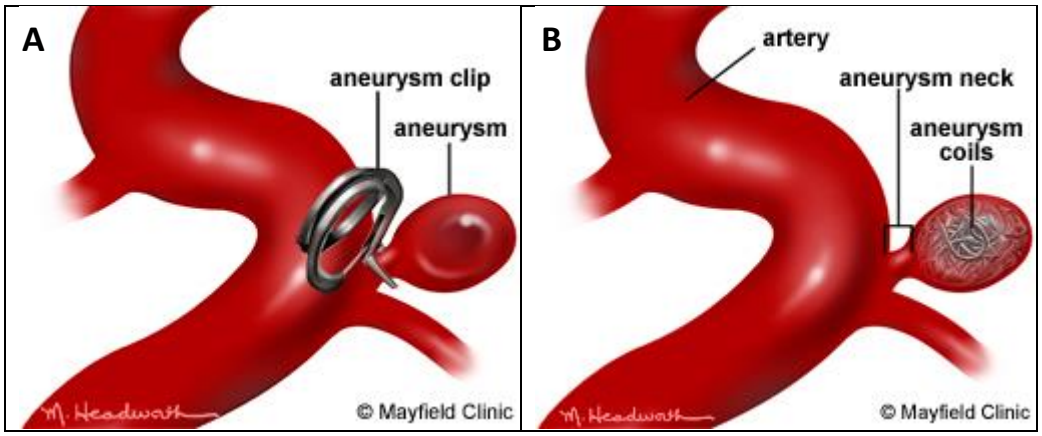

Figure 1.2: A saccular aneurysm (A) surgically treated with an aneurysm clip, and (B) treated with endovascular coil embolization therapy.

Aneurysm clipping requires a high risk, invasive surgery to implant a clip that prevents blood from flowing into the aneurysm sac[21]. Aneurysm location is often a limiting factor in these procedures[22]. Endovascular coiling is a minimally-invasive alternative that aims to fill the aneurysm sac with material to minimize blood flow, induce thrombosis, and promote endothelialization of the aneurysm neck[22-25]. Coiling allows for greater access to tortuous cerebral vasculature and reduces in-hospital mortality[26]. In 1991, soft platinum coils were developed for use as filling material. The procedure involves the delivery of coils through a microcatheter directly into the aneurysm sac with the help of fluoroscopy imaging[27]. Despite some success in small aneurysms (< 4 mm neck diameter), platinum coils are limited by chronic inflammation[28], low volume occlusion (23-37%)[29,30], and recanalization of the aneurysm sac[24,31,32]. Later, polymer coated coils were developed to address some of these issues. Hydrogel coatings on platinum coils resulted in higher volume occlusion (45-85%) but recurrence is still an issue in aneurysms with a neck greater than 8 mm[33-35]. Bioactive or biodegradable polymer coated coils showed promising results initially but exhibited recanalization of the aneurysm sac as the polymer was absorbed by the body[36].

Polyurethane SMP foams have been incorporated into an NED that is well suited for adoption by clinicians in the field because of its similarity to existing devices. The implant portion of the device contains an SMP foam secured onto a platinum wound nickel-titanium (nitinol) backbone wire[10]. The implant is laser welded and epoxied to a pusher wire that enables navigation through the length of the microcatheter and to the aneurysm site. Device features include X-ray visibility, passive actuation at body temperature (37°C), the ability for catheter delivery, and an electrolytic detachment mechanism[10].

1.3. Particulate matter in SMP foams

A particulate is defined by the United States Pharmacopeia (USP) as "mobile undissolved particles, other than gas bubbles, unintentionally present" and can be generated by manufacturing processes or by the breakdown of device components[37,38]. For implantable medical devices, the FDA requires evaluation of the particulates generated by the material, manufacturing processes, and the final assembled device[39,40]. Particulates generated by an implanted device serve as potential emboli for downstream microvasculature[41,42]; un-intended embolization of brain microvasculature has very serious health implications that make particulate characterization a high priority for device evaluators[40,41].

Thus, the total size, geometry, and quantity of particulates is an indication of embolic risk posed by the device[38]. It is unknown whether the SMP foams and foam-based devices generate harmful levels of particulates and there is no existing protocol to quantify or characterize particulate matter in these materials. There are a number of processing steps between synthesis and implantation that could be potential sources of particulate matter. In polyurethane SMP foams, there is a potential for micro-fracture of the struts in the foam matrix, resulting in particulate generation during device fabrication, processing, and delivery[5].

Foam fabrication was carried out using a three step process. First, an isocyanate premix was prepared and allowed to cure for 48 hours. Then, a hydroxyl premix was made by mixing surfactants, catalysts, and hydroxyl groups. Lastly, the isocyanate and hydroxyl premixes were combined with a physical blowing agent and left to cure for at least a week[14]. After foam fabrication, the foam is cleaned through a series of isopropyl alcohol (IPA) and reverse osmosis (RO) water sonications and tumble cycles, mechanically reticulated using a floating array of pins, cut to its desired shape using a biopsy punch, and radially compressed or "crimped" down to its secondary geometry. All of these processes are potential sources for particulates that could pose a threat upon implantation into the brain.

1.4. Techniques for quantification of particulate matter

Currently, there are two primary modes of particulate quantification: light obscuration (LO) and microscopy[37]. Light obscuration is the industrially favored technique because it allows for automated particulate quantification at a rapid and repeatable rate[44]. Microscopy evaluation involves manually counting particulates using a light microscope and a calibrated micrometer[44]. This work focuses on the utilization of LO to quantify particulates generated by polyurethane SMP foams and foam devices in order to effectively evaluate the embolic risk posed by these SMP embolization devices.

1.4.1. Light obscuration

Particulate quantification and sizing using LO is performed with a particle counter device. The particle counter consists of an optical sensor and specifically programmed counting electronics[45]. The sensor contains a 780 nm infrared laser diode that converts light energy into electrical voltage outputs. As a sample solution is flowing through the sensor, it disrupts a portion of the light and produces an electrical pulse proportional to its size; pulse

amplitude corresponds to particle size as shown in **Figure 1.3**[45]. The device groups the particles into size bins and provides the quantity of particles in a given sample solution for each size bin.

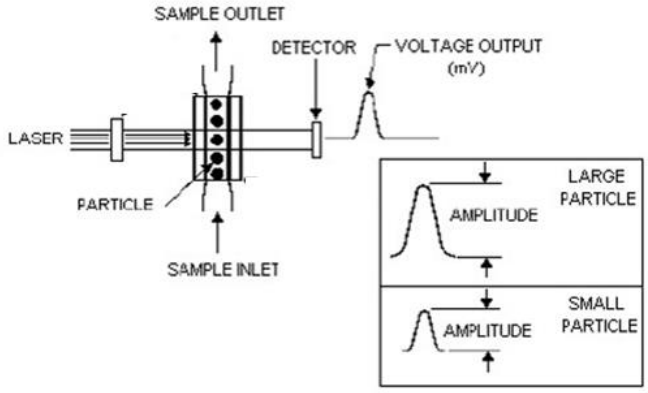

Figure 1.3: Schematic of light obscuration (LO) flow cell on particle counter device.

Sample preparation is done according to the type of sample being analyzed. In general, it is based upon a protocol outlined in USP 788, a guidance document for particulate analysis of parenteral injections. The protocol outlines acceptable thresholds for "particle free" water that can be used during testing, and provides a method for sample agitation. LO particle counters are limited in analysis of certain sample types. Organic particles cannot be quantified with accurate resolution because their index of refraction is close to that of water, causing them to reflect more light and be recorded in a size range several microns below their actual size[45]. To address this discrepancy, size bins are used instead of exact sizes. Additionally, highly viscous solutions are generally not suitable for this method.

1.4.2. Microscopy

Particulate analysis *via* microscopy is performed manually on a binocular microscope. Sample solutions are passed through a filter assembly and examined on a membrane filter. Once the particulates have been isolated by the filter, they are manually sized and quantified by the operator with an ocular micrometer. This method is limited by the time needed to perform each count and the operator's ability to accurately and consistently group the particles into the appropriate size ranges. It is not a feasible evaluation approach for a large scale manufacturer that needs to evaluate large numbers of samples. However, the method is compatible with highly viscous solutions that are not suitable for use with light obscuration methods.

1.5. Summary of thesis

Determination of the size and number of particulates generated by polyurethane SMP foams is required in their development as embolic materials in biomedical applications. The goal of this thesis is to develop protocols for measuring and characterizing particulate matter in SMP foams and SMP foam-based devices.

Chapter II discusses the approach to quantify particulate matter after cleaning and reticulation processes as well as testing the cytocompatibility of uncleaned, nanoparticle-loaded, polyurethane SMP foams using light obscuration. Particulate levels from cleaned foams were compared to uncleaned foams to assess the efficacy of the current cleaning process. Two reticulation processes are compared and evaluated on the basis of particle generation, and concentrated particulate solutions were taken from representative foam samples and administered to fibroblasts to assess cytocompatibility of particulates. The methods for particulate analysis and cytocompatibility testing are described, and the results are presented.

Visual characterization of particulates using a scanning electron microscope (SEM) was performed to report on particulate geometry in addition to their size and number to fully assess their potential embolic risk. The method for preparation of the SEM samples and identification of the particulates is described and the results are discussed.

Chapter III discusses the analysis of the particulates generated by foam-based devices delivered into a straight tube and tortuous model. Particulate analysis was performed on SMP foam devices during delivery into two flow loops of increasing tortuosity. The flow systems were developed to simulate delivery into a blood vessel at physiologic temperatures and tortuosity.

CHAPTER II

PARTICULATE ANALYSIS OF VARIOUS PROCESSING STEPS FOR SHAPE MEMORY POLYMER FOAMS FOR ANEURYSM OCCLUSION[*]

2.1 Introduction

When evaluating particulate generation of a material intended for implantation, each step in the manufacturing and preparation process must be considered and examined as a potential source for particulates[41]. A technical information report (TIR) from the Association for the Advancement of Medical Instrumentation (AAMI) advises testing for particulates generated during manufacturing, packaging, acute application, sterilization, and degradation[39]. The FDA has yet to define specific tests detailing acceptable particulate limits for medical devices, but they strongly recommend measuring the size and quantity of particulates that a device may generate as an indication of the embolic risk that the device will pose[38,41]. The U.S. Pharmacopeial Convention's chapter 788, "Particulate Matter in Injections" is commonly referenced when evaluating particulates[37]. It provides a protocol for counting particulates in solution and quantitative limits for particles $\geq$10 μm and $\geq$25 μm. However, the chapter does not outline a protocol for evaluating particulates generated by medical devices or provide acceptable thresholds for particle generation. To this end, an appropriate protocol should be developed to ensure that the particles will be in suspension during evaluation.

[*] Figure 2.10 in this chapter is reprinted with permission from "Modification of shape memory polymer foams using tungsten, aluminum oxide, and silicon dioxide nanoparticles" by S. Hasan, R. Thompson, H. Emory, A. Nathan, A. Weems, et al., 2016. *Royal Society of Chemistry Advances, **6**: 918 – 927, Copyright 2016 by Royal Society of Chemistry.*

This thesis evaluates the particulate generation in SMP foams that serve as candidates for an NED. The foams are synthesized with varied monomer ratios and filler types, weight percentages (wt%), and volume percentages (vol%) to enable tailoring of the foam's physical and mechanical properties. Fillers are incorporated to improve Young's modulus and tensile strength of the foams[6]. Varying the monomer concentrations affects the hydrophobicity of the low density foams, and varying the weight and volume percentages of the fillers allows finer control of foam mechanical properties[5,47]. This thesis aims to provide quantitative feedback on the particulates generated from the foams when subject to cyclic inversion testing, cleaning, and two different reticulation processes. Furthermore, 3T3 fibroblast viability is assessed upon administration of concentrated particulate solutions.

2.2. Materials and methods

2.2.1. Particle counter validation

Validation of the particle counting system was performed by introducing a known size and quantity of calibrated microspheres (Count-Cal, Thermo Fisher Scientific, Waltham, MA) into the particle counter and ensuring that it outputted at least 75% of the particles introduced into the system. Microspheres 15 µm in diameter and at a concentration of 1500 particles per mL were used for this validation. The microspheres were suspended in 50 mL of solution; each test run consisted of manual inversion of the container 10 times followed by quantification of the particles contained in 10 mL of microsphere suspension. This sampling method allowed 4 test runs per 50 mL sample.

2.2.2. Materials

N,N,N',N'-tetrakis(2-hydroxypropyl)ethylenediamine (HPED, 99%; Sigma-Aldrich Inc., St. Louis, MO), triethanolamine (TEA, 98%; Sigma-Aldrich Inc., St. Louis, MO),

trimethyl-1,6-hexamethylene diisocyanate, 2,2,4- and 2,4,4-mixture (TMHDI; TCI America Inc., Portland, OR), hexamethylene diisocyanate (HDI; TCI America Inc., Portland, OR), DC 198 (Air Products and Chemicals Inc., Allentown, PA), DC 5943 (Air Products and Chemicals Inc., Allentown, PA), T-131 (Air Products and Chemicals Inc., Allentown, PA), BL-22 (Air Products and Chemicals Inc., Allentown, PA), Enovate 245fa Blowing Agent (Honeywell International Inc., Houston, TX), 2-propanol 99% (IPA) (VWR, Radnor, PA) and deionized (DI) water (E-Pure water system, Barnstead International, Dubuque, IA) were used as received. Tungsten nanoparticles (W, 99.95%, 40-60 nm; US Research Nanomaterials Inc., Houston, TX), aluminum oxide nanoparticles (Al_2O_3, alpha, 99+%, 80 nm, hydrophilic; US Research Nanomaterials Inc., Houston, TX), and silicon dioxide nanoparticles (SiO_2, 98+%, 60-70 nm, amorphous; US Research Nanomaterials Inc., Houston, TX) were dried under vacuum at 90° C for 12 hours prior to foam synthesis[5].

Penicillin/streptomycin (P/S, 1%; VWR, Radnor, PA), Dulbecco's modified eagle medium (DMEM; VWR, Radnor, PA), newborn calf serum (NBCS, 10%; Sigma-Aldrich Inc., St. Louis, MO), fungizone (0.1%, VWR, Radnor, PA), calcium chloride ($CaCl_2$, 0.1%; Sigma-Aldrich Inc., St. Louis, MO), formaldehyde (0.5%; Sigma-Aldrich Inc., St. Louis, MO), acetic acid (1%; Sigma-Aldrich Inc., St. Louis, MO), ethanol (50%; Sigma-Aldrich Inc., St. Louis, MO), 3T3 fibroblasts (ATCC, Manassas, VA), and a neutral red (NR) uptake assay (TOX4, Sigma-Aldrich Inc., St. Louis, MO) were used as received.

2.2.3. Foam synthesis

Twenty different variations of SMP foams, shown in Table 1, were synthesized using the three-step protocol previously described by Hasan *et al.*[5,48]. Isocyanate pre-polymer were synthesized using appropriate molar ratios of HPED, TEA, TMHDI, and HDI, with a 35 wt%

hydroxyl (OH) composition. Nanoparticles were physically incorporated into the isocyanate pre-polymers *via* high shear mixing prior to foam blowing at the appropriate concentrations. A OH mixture was prepared with the remaining molar equivalents of HPED and TEA, along with catalysts, surfactants, and DI water. During foam blowing, a physical blowing agent, Enovate, was mixed with the isocyanate pre-polymer and the OH mixture using a speedmixer (SpeedMixer, FlakTek Inc., Hauschild, Germany). The resulting foams were cured in a vacuum oven at 90° C for 20 minutes. The SMP foam nanocomposites were cooled to room temperature (21 ± 1° C) followed by a 24-hour cold cure before further processing.

SMP foams synthesized with 100% TMHDI and no fillers were used as controls. Eleven foams were synthesized containing either Al_2O_3 or SiO_2 fillers with varied monomer ratios, as listed in Table 1. The two isocyanate monomers used were TMHDI and HDI. The remaining eight foams were synthesized with varying weight or volume percentages of W filler. Weight percentages ranged from 0.5 – 3 %, as an unfavorable decrease in mechanical properties is exhibited by foams with higher wt% fillers (> 3 %)[5]. Additionally, 3, 5, 6, and 8 vol% W foams were assessed, due to the increased X-ray visibility exhibited by these foams[48]. **Table 2.1** details the compositions of the foams synthesized.

Table 2.1: Filler type, monomer ratio, and weight or volume percentage used in foam syntheses.

Foam Name	Monomer Ratio	Filler Particle	Filler Weight %	Filler Volume %
Control	100% TMHDI	---	---	---
50:50 1 wt% Al_2O_3	50% HDI 50% TMHDI	Al_2O_3	1	---
20:80 1 wt% Al_2O_3	20% HDI 80% TMHDI	Al_2O_3	1	---
0.5 wt% Al_2O_3	100%TMHDI	Al_2O_3	0.5	---
0:100 1 wt% Al_2O_3	100% TMHDI	Al_2O_3	1	---

Table 2.1 Continued

Foam Name	Monomer Ratio	Filler Particle	Filler Weight %	Filler Volume %
2 wt% Al_2O_3	100% TMHDI	Al_2O3	2	---
3 wt% Al_2O_3	100% TMHDI	Al_2O_3	3	---
4 wt% Al_2O_3	100% TMHDI	Al_2O_3	4	---
5 wt% Al_2O_3	100% TMHDI	Al_2O_3	5	---
0.5 wt% SiO_2	100% TMHDI	SiO_2	0.5	---
1 wt% SiO_2	100% TMHDI	SiO_2	1	---
2 wt% SiO_2	100% TMHDI	SiO_2	2	---
0.5 wt% W	100% TMHDI	W	0.5	---
1 wt% W	100% TMHDI	W	1	---
2 wt% W	100% TMHDI	W	2	---
3 wt% W	100% TMHDI	W	3	---
3 vol% W	100% TMHDI	W	---	3
5 vol% W	100% TMHDI	W	---	5
6 vol % W	100% TMHDI	W	---	6
8 vol % W	100% TMHDI	W	---	8

2.2.4. Cleaning process

Foams were subject to a cleaning process aimed towards removing any residual chemicals from foam synthesis, washing out any weak or damaged foam struts, and removing any environmental contaminants that may have been introduced during post-synthesis processing. The process involves two 15-minute IPA sonications, followed by a 5-minute tumble cycle, and four 15-minute RO water sonications. The foams were then submerged in RO water, and placed in a -2° C freezer for 12 hours. Lastly, the foams were placed in a freeze dryer (Freezone 6, Labconco Corporation, Kansas City, MO) for 12 hours at 25° C.

2.2.5. Reticulation

Foams were subject to reticulation in order to remove or puncture the thin membranes between foam struts within the SMP foam matrix[49]. Reticulation is done to allow for better infiltration of blood into the foam matrix, and to improve its potential for healing once implanted into the aneurysm sac[49,50]. Mechanical and plasma reticulation methods were evaluated on the basis of particulate generation. The two reticulation methods were compared against a control foam composed of 100% TMHDI and containing no filler particles.

2.2.5.1 Mechanical reticulation

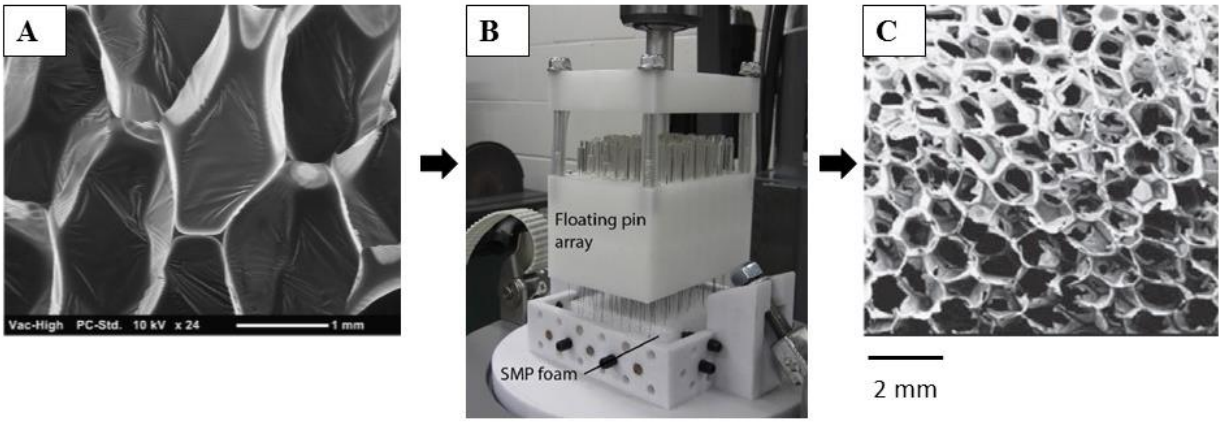

Figure 2.1: SEM images of (A) SMP foam prior to reticulation, (B) the mechanical reticulation setup, and (C) SMP foam post-reticulation.

The mechanical reticulation system includes a gravity-driven floating nitinol pin array, and a vertically oscillating vibratory shaker (**Figure 2.1**)[49]. Foam samples were cut to rectangular blocks 30 mm in height and 5 cm in length/width and then subject to the cleaning protocol outlined in Section 2.4. The foam blocks were held in place by custom vibratory mounting platform that is cyclically raised and lowered for a duration of 2.5 hours. Then, the foam block was turned over, re-secured, and subject to another reticulation cycle lasting 2.5

hours. Complete reticulation of both sides of the foam block took 5 hours. Two foam blocks of 100% TMHDI foam with no filler were mechanically reticulated, cut into nine 8 mm cylinders 30 mm (n = 10) in length using a biopsy punch (Acu-punch, Acuderm Inc., Ft. Lauderdale, FL), and subject to particulate analysis.

2.2.5.2 Plasma reticulation

Plasma reticulation is a diffusive process where plasma reactive species rupture open and volatizes cell membranes at the surface of the foam[51]. As cell membranes at the surface are ruptured, the reactive species are able to access membranes further inside the foam matrix, allowing for reticulation of the entire foam sample[51]. Nine 100% TMHDI foam cylinders 8 mm in diameter and 30 mm in length were cleaned using the protocol outlined in Section 2.4 and then reticulated using a cold plasma treatment system (Aurora 0350 Plasma Surface Treatment System, Plasma Technology Systems, Belmont, CA). Power was set to 300 watts, gas flow rates were 800|200 for $O_2|CF_4$, and the cycle duration was 3 minutes[51]. Once reticulated, the samples were subject to particulate analysis.

2.2.6. Cyclic inversion testing of particulate generation

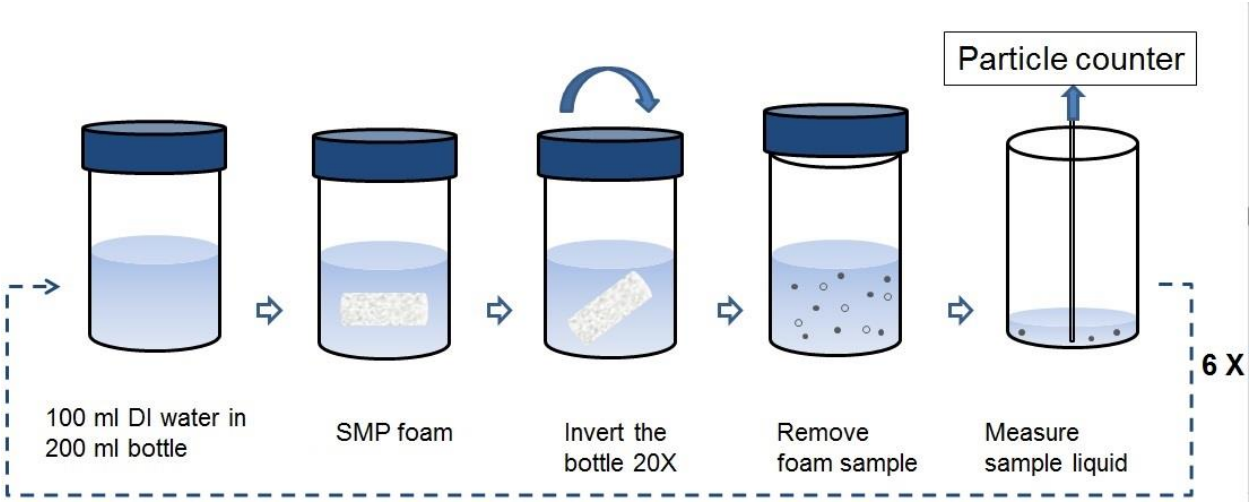

Figure 2.2: Schematic representation of the cyclic wash protocol used to evaluate uncleaned foam samples for particulate generation.

Foam cylinders (n = 5) with 8 mm diameter and 3 cm length were cut from the twelve foam formulations (**Table 2.1**) using an 8 mm biopsy punch. Particulate data was collected for three distinct size ranges: ≥10 μm, ≥25 μm, and ≥50 μm, as recommended by the FDA. A procedure was developed for agitation of the foam samples in reference to USP 788. Briefly, foam sample agitation was achieved by successive inversion of a single foam cylinder 20 times in DI water. The resulting particulate levels in the DI water were measured using light obscuration (PC5000, Chemtrac Inc., Norcross, GA). Particle counts from the SMP foams were then compared to the limits for small volume infusions stated in USP 788 (**Table 2.2**) to characterize the foams on the basis of particulate generation.

Table 2.2: USP 788 Acceptable limits for injection or parenteral infusion[37].

Volume	Particle Size Range	Acceptable Number of Particles
≤ 100 mL	≥ 10 µm	6000
≤ 100 mL	≥ 25 µm	600

As shown in **Figure 2.2**, each SMP foam cylinder was placed in a bottle containing 100 mL DI water, agitated, removed from the water. This process constituted one inversion cycle. For cleaned foams, the suspension of particles was analyzed using the particle counter at this point. Uncleaned foam samples, however, were placed into a subsequent bottle of fresh DI water and subject to more inversion cycles. Each uncleaned sample was subjected to six inversion cycles or the number of cycles required to reach a plateau in the level of particulate generation (92 ± 3% decrease). Decreases in particulates from cycle to cycle were quantified using the following formula:

$$Percent\ Decrease = \frac{N_{n-1} - N_n}{N_{n-1}}\ x\ 100\%$$

where N is the number of particulates, and n is the cycle number. Due to the high sensitivity of the particle counter, baseline water counts were taken prior to each experiment to ensure that the DI water used met the criteria outlined in USP 788 (i.e., for water to be deemed particle-free, it must contain less than 1 particle ≥ 10 µm in size per mL)[37].

2.2.7. Visual characterization

Visual characterization was performed to determine the geometries of particulates in all three ranges recorded (≥10 µm, ≥25 µm, and ≥50 µm). Control foams (100% TMHDI, no filler), 1 wt% Al_2O_3 filler foams, 1 wt% SiO_2 filler foams, 1 wt% W filler foams, and 3 vol% W filler foams were mechanically agitated to purposefully generate particulates. The

particulates were collected on an SEM mount containing carbon-tape and then placed under vacuum at 25° C for 48 hours. Then, the samples were sputter coated with a gold sputter coater (Cressington Sputter Coater, Ted Pella Inc., Redding, CA) for a duration of 60 seconds at a pressure of 20 mBar and imaged using a SEM (Neoscope JCM-5000, Jeol Inc., Peabody, MA).

2.2.8. Cytocompatibility assay

Control foams (100% TMHDI, no filler), 1 wt% Al_2O_3 filler foams, 1 wt% SiO_2 filler foams, 1 wt% W filler foams, and 3 vol% W filler foams were subject to cyclic inversion with DI water according to the protocols outlined in Section 2.5. Forty mL of particulate solution was collected after the first and sixth cycles for each sample, and 40 mL of fresh DI water was collected as a control. P/S was added to each solution at 1% between collection and cell treatment to reduce contamination. The solutions were centrifuged for 10 min at 4400 rpm to pellet particulates; then, the supernatant was aspirated and exchanged for 2 mL of cell culture media to make 20x concentrated particulate solutions. Cell culture media was composed of DMEM, 10% NBCS, 1% P/S, and 0.1% fungizone.

3T3 fibroblasts were seeded in 96-well tissue culture plates at a concentration of 5,000 cells/well and incubated in a humidified incubator at 37°C with 5% carbon dioxide (CO_2) for 24 hours. Cell morphology was observed in all wells using a Nikon Eclipse TE 2000-S inverted microscope (Nikon, Melville, NY) and even cell distribution was confirmed before addition of the treatments. Cell culture media was aspirated from the wells, and 200 μL of the designated treatment solutions were added to each well. Cells were incubated with particulate treatments for 48 hours at 37°C with 5% CO_2.

Following incubation, cell morphology was observed in all wells using the Nikon inverted microscope to qualitatively evaluate changes induced by addition of the treatments.

The extract treatments were then removed and a NR uptake assay was utilized to quantify cell viability. NR is a red dye that is actively transported across the cell membrane where it accumulates within lysosomes[52]. After incubation with NR for 3 hours, the cells were fixed with a solution of 0.1% $CaCl_2$ in 0.5% formaldehyde. The dye was solubilized in a solution of 1% acetic acid in 50% ethanol for measurement. A plate reader (Tecan Infinite M200 Pro, Morrisville, NC) was used to measure the optical density at 540 nm to quantify the amount of remaining dye in each well. Cell viability is expressed as a percentage using the following equation:

$$Cell\ Viability\ (X) = \frac{OD_{540}(X)}{OD_{540}(Negative\ Control)}$$

where X is any treatment group and the negative control for cytocompatibility (DI water) is used as a standard that equals 100% viability.

2.2.9. Statistical calculations

Data was compiled and expressed as mean ± standard deviation (SD) (Table 3), and statistical analysis was performed using Student's t-tests (Microsoft Excel, Microsoft, Redmond, Wash). The 12 foam compositions were divided into sub-groups and compared with other foams in their sub-group to determine statistical differences in particulate generation with a 95% confidence level ($p < 0.05$). The particulates $\geq$10 μm generated after the first wash were found to be most characteristic of the foam compositions. For this reason, first wash particulate levels were used when performing the t-tests.

2.3. Results and discussion

2.3.1. Particle counter validation

Introduction of the calibrated microspheres into the particle counter returned that the particle counter used is capable of recording at least 75% of the particles introduced into the

system. **Table 2.3** shows that the average particle levels over 8 runs was 11,493 ± 243 signifying 76.6% recovery. These results validate the use of the Chemtrac particle counter as a device capable of accurately measuring particles in this size range.

Table 2.3: Size and quantity of microspheres inputted, acceptable value for ≥75% recovery, and the average ± standard deviation of particle levels outputted by the particle counter.

Input Microsphere Size (μm)	Input Microsphere Number	Output Size Range (μm)	Chemtrac Output (Acceptable Value)	% Recovery
15	15,000	10 – 25	11,493 ± 243 (11,250)	76.6

2.3.2. Analysis of uncleaned foams

All uncleaned foam types generated the highest average number of particulates after the first inversion cycle, and the average number of particulates declined exponentially with each subsequent cycle. The magnitude of generated first-cycle particulates varied with foam composition, with the control foam generating the lowest number of particulates of the tested foam compositions. All of the foams tested exhibited a decrease in all three particulate size ranges after their initial cycle. On average, there was an 85 ± 6% decrease in particulates ≥10 μm and ≥25 μm after the first cycle (Table 3). Subsequently, a 47 ± 14% decrease was observed between the second and third cycles. This trend was observed with all foam chemistries. Quantification of decreases in particulates observed after the first and second washes and average particulate counts for particles ≥10 μm and ≥25 μm are shown in **Table 2.4**. Particulate counts for particles ≥50 μm were very low (max of 0.17 particles per mL) and exhibited no discernable trends (**Figure 2.7**). The results from NR uptake assay supported the cytocompatibility of particulates generated from all tested foam compositions.

Table 2.4: Mean ± standard deviation of particulate numbers from the first cycle, and percent decrease after 1st and 2nd cyeles for particles ≥ 10 μm and ≥ 25 μm.

Foam (N = 5)	Mean Particulates ≥10 μm	Mean Particulates ≥25 μm	Mean % Decrease after 1st cycle	Mean % Decrease after 2nd cycle
Control	760 ±140	70 ± 20	80 ± 10	50 ± 30
50:50 1 wt% Al_2O_3	1470 ± 550	83 ± 40	70 ± 20	30 ± 25
20:80 1 wt% Al_2O_3	2300 ± 520	260 ± 330	90 ± 5	50 ± 40
0:100 1 wt% Al_2O_3	1470 ± 860	50 ± 20	70 ± 20	35 ± 30
1 wt% SiO_2	1100 ± 240	40 ± 20	80 ± 15	45 ± 30
1 wt% W	800 ± 220	40 ± 10	90 ± 10	30 ± 20
2 wt% W	1070 ± 350	60 ± 20	90 ± 5	50 ± 25
3 wt% W	1140 ± 550	30 ± 10	75 ± 10	45 ± 30
3 vol% W	1430 ± 460	130 ± 60	80 ± 10	50 ± 25
5 vol% W	1380 ± 320	90 ± 40	90 ± 5	60 ± 10
6 vol% W	1480 ± 440	130 ± 110	90 ± 5	55 ± 30
8 vol% W	2080 ± 460	120 ± 100	85 ± 10	65 ± 30

2.3.2.1. Effects of monomer ratio

Particulate analysis of foams with varied monomer ratios of HDI to TMHDI (50:50, 20:80, 0:100) revealed that foams containing a 20:80 HDI:TMHDI ratio (**Figure 2.3**) generated the highest number of particulates after their first inversion cycle. T-tests were performed to quantify differences in particulate generation in relation to monomer ratios. There was a statistically significant difference between the 20:80 HDI:TMHDI and the 50:50 HDI:TMHDI foams ($p = 0.02$) for ≥10 μm particle generation (**Figure 2.3A**). By increasing the ratio of TMHDI, the more hydrophobic of the two monomers, the foams become stiffer due to the reduced rate of water permeation into the foam matrix[47]. This increased stiffness could be the

cause of higher particulate levels in the foams with higher TMHDI ratios. There were no significant differences exhibited in the ≥25 µm size range (**Figure 2.3B**).

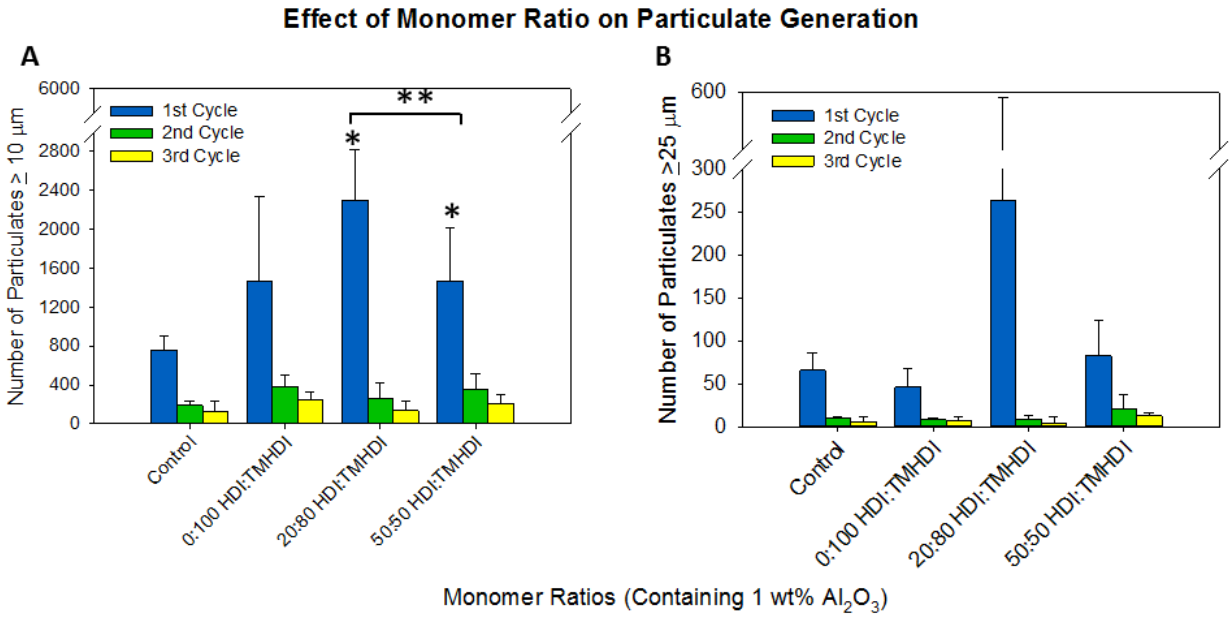

Figure 2.3: Numbers of particulates (A) ≥10 µm and (B) ≥25 µm from 1 wt% Al_2O_3 foams with varying monomer ratios of 50:50 HDI:TMHDI, 20:80 HDI:TMHDI, and 100% TMHDI. n = 5; mean ± standard error displayed; *p < 0.05 relative to control; **p < 0.05 between the bracketed groups. USP 788 limit for particulates ≥10 µm = 6000; limit ≥25 µm = 600.

2.3.2.2. Effects of filler type

Variation in filler type resulted in differences in first cycle particulate generation (**Figure 2.4**). Of the three fillers, foams with W generated the lowest number of first cycle particulates and foams with Al_2O_3 produced the highest number of particulates. T-tests were performed to assess differences in particulate generation among the filler particles. Statistical analysis returned that the only significant difference ($p < 0.05$) was between the SiO_2 foams and the W foams ($p = 0.04$) (**Figure 2.4A**). In general, adding fillers at low concentrations increased the small particulates (>10 µm) but reduced the larger (>25 µm) particulates. Filler incorporation reinforces the polymer matrix and, at low concentrations (0.5 – 1%), provides

physical net points that allow for improved resistance to mechanical deformation[5]. The SiO_2 foam most likely differed from the control foam because of the lower mass of the SiO_2 nanoparticles relative to the W and Al_2O_3 nanoparticles; due to this reduced mass, a higher number of SiO_2 nanoparticles were required to achieve the same weight percent loading as the W and Al_2O_3 loaded foams[5]. The increased numbers of ≥10 µm particulates (**Figure 2.4A**) seen in the filler foams relative to the control foam could be due to less stable areas of the foam with aggregates of filler nanoparticles, and the reduced numbers of ≥25 µm particulates (**Figure 2.4B**) could be related to the increased net points that the fillers provide.

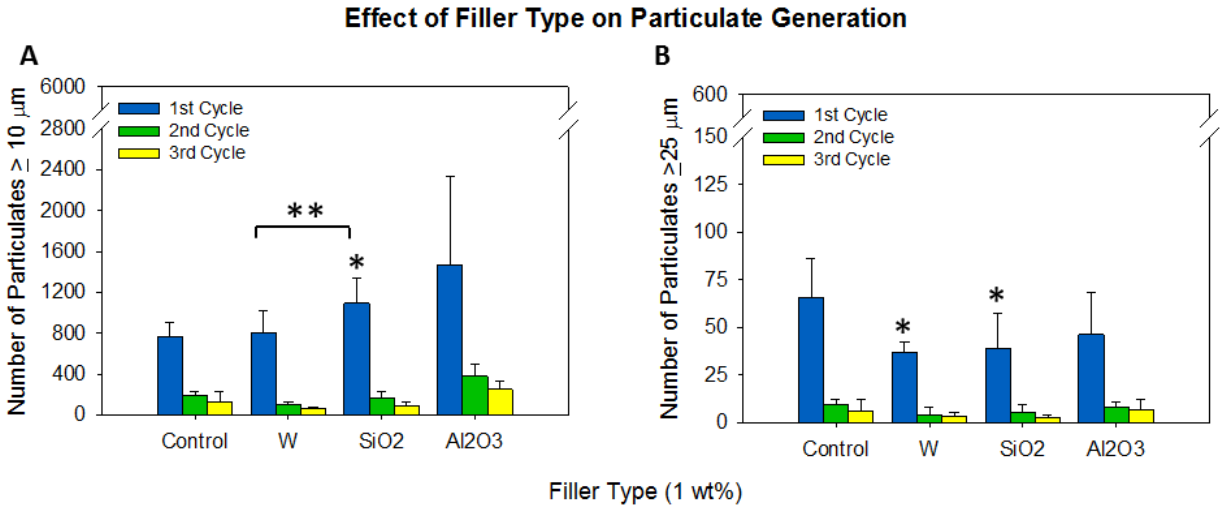

Figure 2.4: Numbers of particulates (A) ≥10 µm and (B) ≥25 µm from foams with W, SiO_2, and Al_2O_3 filler types. n = 5; mean ± standard error displayed; *p < 0.05 relative to control; **p < 0.05 between bracketed groups. USP 788 limit for particulates ≥10 µm = 6000; limit ≥25 µm = 600.

2.3.2.3. Effects of filler weight percent

Variation in the weight percentage of W incorporated into the foam resulted in differences in particulate generation (**Figure 2.5**). Statistical analysis returned that the only significant difference ($p < 0.05$) was between the 2% W foams and the 3% W foams ($p = 0.03$)

in the ≥25 µm size range (**Figure 2.5B**). The average magnitude of generated particulates ≥10 µm recorded after the first inversion cycle generally increased as weight percentage W was increased (**Figure 2.5A**). However, T-tests returned that the number of generated particulates ≥10 µm did not differ significantly for the three weight percentages tested despite the observed positive correlation. The relatively low filler concentrations tested here were previously shown to have improved foam toughness and lowered particulate levels[5]. Thus, particulate levels that were generally less than or equal to the control foam was expected.

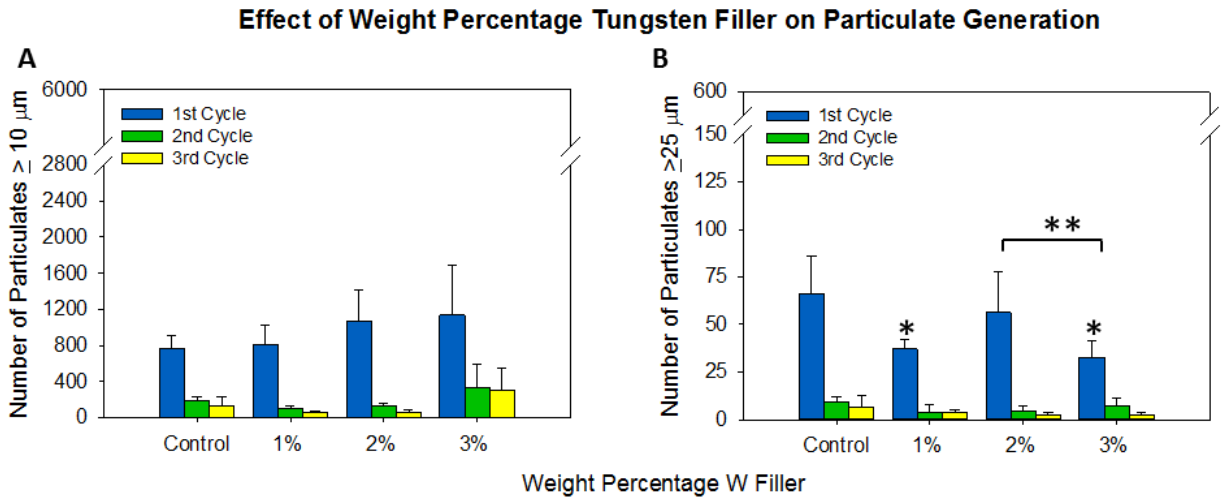

Figure 2.5: Numbers of particulates (A) ≥10 µm and (B) ≥25 µm from foams with varying weight percentages of W. n = 5; mean ± standard error displayed. USP limit for particulates ≥10 µm = 6000; limit ≥25 µm = 600.

2.3.2.4. Effects of filler volume percent

Variation in volume percentage of W incorporated into the foam also resulted in differences in first cycle particulate generation (**Figure 2.6**). T-tests showed that the 8 vol% W generated a statistically higher number of particulates than the 3, 5, and 6 vol% W foams ($p < 0.05$) in the smaller size range (**Figure 2.6A**). Despite the weak positive correlation demonstrated between increasing vol% and particulate levels (**Figure 2.6A**), none of the 3, 5,

or 6 vol% W foams differed significantly from one another. Increased filler concentrations (> 4 vol%) were previously seen to lower material toughness[48] and, as observed in this study, generated higher particulate levels in both the ≥10 µm and ≥25 µm size ranges (**Figure 2.6A and 2.6B**). High filler content decreases foam stiffness due to disruption of the foam matrix when filler aggregates replace the polymer within the foam struts and, ultimately, makes the foams more susceptible to brittle fracture[48].

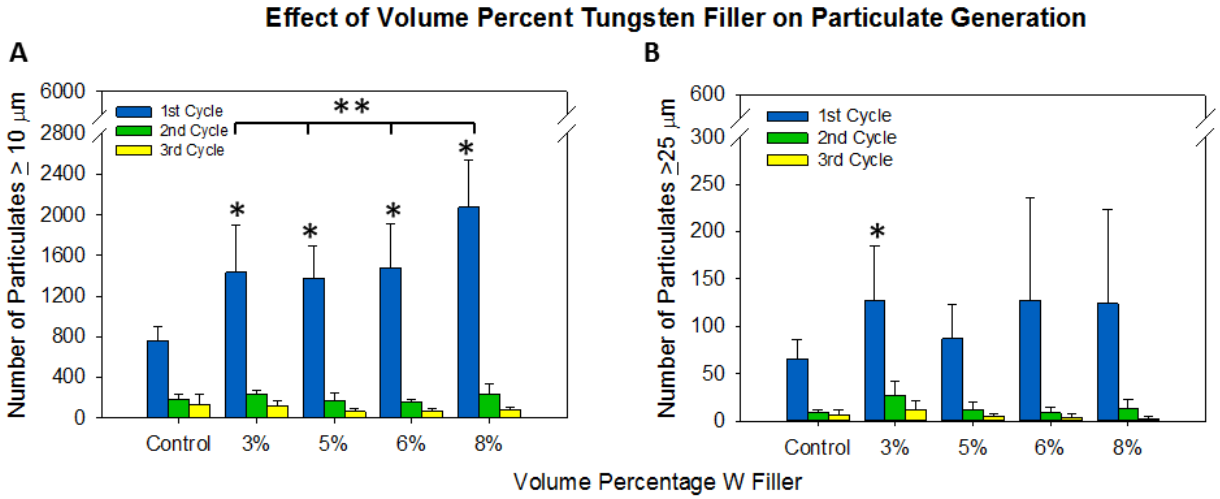

Figure 2.6: Numbers of particulates (A) ≥10 µm and (B) ≥25 µm from foams with varying volume percentages of W. n = 5; mean ± standard error displayed; *p < 0.05 relative to control; **p < 0.05 between bracketed groups. USP 788 limit for particulates ≥10 µm = 6000; limit ≥25 µm = 600.

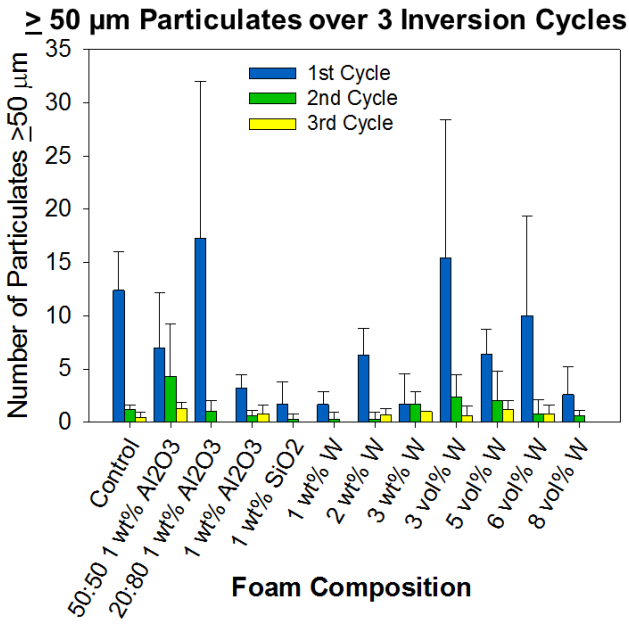

Figure 2.7: Particulates ≥ 50 µm generated over 3 cyclic inversion cycles for all foam chemistries tested. n = 5; mean ± standard deviation displayed. No USP or FDA limit for particulates ≥ 50 µm.

2.3.2.5. Visual characterization of foams

Visual characterization of particulates from 1 wt% Al_2O_3, 1 wt% SiO_2, 100% TMHDI, and 4 vol% W foams showed that the particulates were fragments of foam struts or foam-cell membranes. **Figure 2.8** shows SEM images of various size particles generated from SMP foam cylinders. The average lengths and widths for the particles displayed in **Figure 2.8** are (L x W): (**A)** 21 x 9 µm, (**B)** 53 x 40 µm, (**C)** 98 x 57 µm, and (**D)** 425 x 67 µm. Characterizing the shape allows us to better assess the embolic risk associated with the particles. Larger particulates (>50 µm) typically had length to width ratios greater than those seen in smaller particulates (<50 µm with length to width ratios approximately 1:1). Non-uniform particles produce greatest risk of invoking the inflammatory response and causing complication during embolization[53].

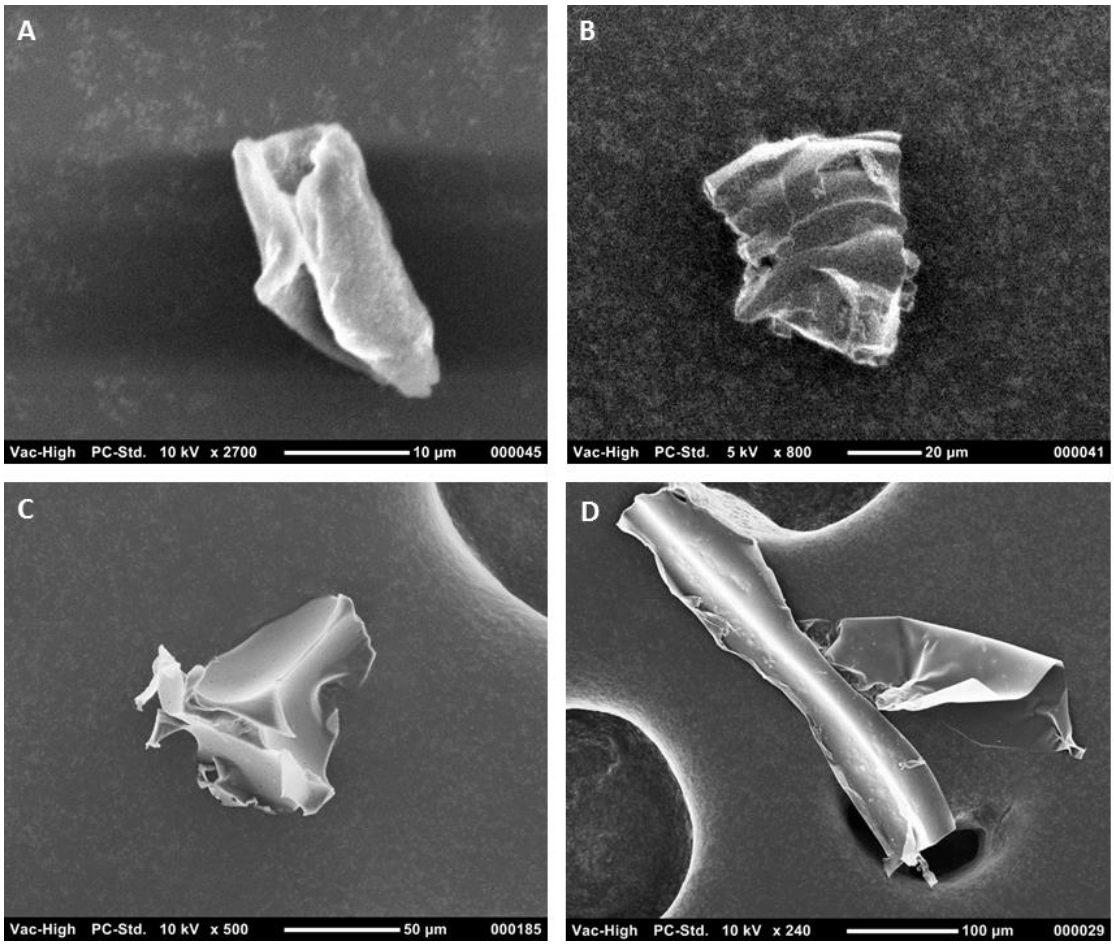

Figure 2.8: SEM images of various sizes of particulates generated from the bulk SMP foam materials at (A) 10 µm, (B) 20 µm, (C) 50 µm, and (D) 100 µm scales.

2.3.2.6. Cytocompatibility assay

The results of the NR uptake assay are shown in **Figure 2.9**. No morphologic changes were observed after 48 hours of incubation with particulate solutions. Cell viability greater than 100% was observed for all treatment groups and ranged from 107% to 117%. This evidence supports the cytocompatibility of all particulate samples. Means compared using Student's t-tests and no statistically significant differences were observed in viability between cycles 1 and 6 for any group.

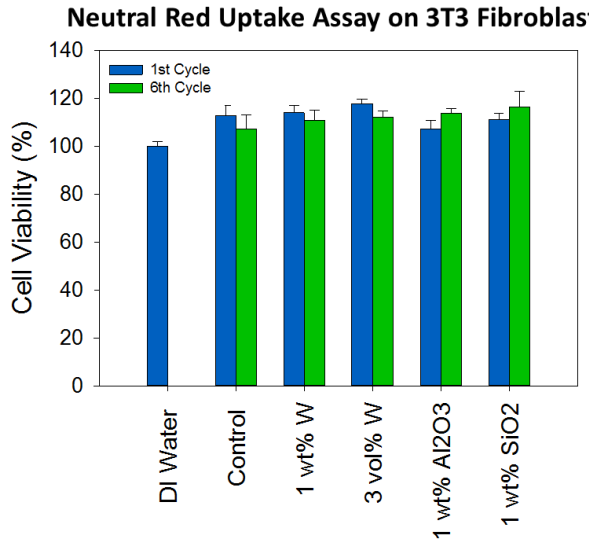

Figure 2.9: Cell viability of 3T3 Fibroblasts determined by Neutral Red Uptake Assay. n = 5; mean ± standard error displayed. No significant differences were observed between the treatment groups.

2.3.3. Particulate analysis of cleaned foams

Quantification of particulate matter in cleaned foams is displayed in **Figure 2.10**. All of the foam chemistries tested exhibited particulate levels below the thresholds stated in USP 788 for particles ≥10 µm (**Figure 2.10A**) and ≥25 µm (**Figure 2.10B**) (Limit ≥10 µm = 6000, limit ≥25 µm = 600). Cleaned foams exhibited significantly lower ($p < 0.05$) levels of particulates than the uncleaned foams. On average, cleaned foams exhibited particulate levels that were 55 ± 15% lower than those of the uncleaned foams.

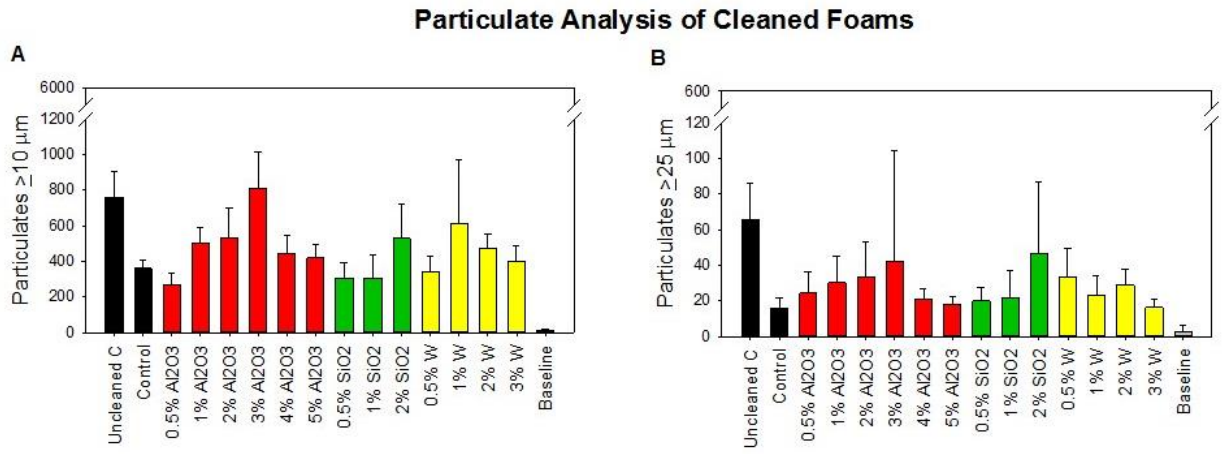

Figure 2.10: Number of particulates (A) ≥10 µm and (B) ≥25 µm for 14 different compositions of cleaned SMP foams. USP 788 limit for particulates ≥10 µm = 6000; limit ≥25 µm = 600.

2.3.4. Particulate analysis of reticulation methods

Different reticulation modalities recorded differing levels of particulate matter in 100% TMHDI foams containing no filler particles (**Figure 2.11**). Both reticulation modalities generated statistically significantly higher ($p < 0.05$) levels of particulates ≥10 µm than those recorded in the control foams. Although mechanical reticulation generated higher levels of particulates than did plasma reticulation, the difference in particulate levels was not statistically significant. There were no statistical differences observed between the processes in the ≥25 µm size range.

Differences between the two reticulation modalities are likely due to a number of factors. First, the mechanical reticulation process involves much higher mechanical stresses and friction forces on the foam due to the nature of the process. Second, since the mechanical process requires physical perforation of the membranes using nitinol wires with higher mechanical properties than the foams being reticulated, there is more damage done to the foam matrix. Third, the 5-hour duration of the process entails that the foams are subject to these

higher mechanical stresses for a substantially longer period of time than the plasma processes. With plasma reticulation, enough energy is generated within the plasma chamber to cause a controlled burning of the foam membranes. This means that the foam struts are subject to minimal mechanical forces during the brief 3-minute process. The difference between the plasma reticulated foams and the control foams is most likely due to the fact that, although the plasma reticulated foams are subject to minimal mechanical forces, the controlled burning of the membranes causes a marginal decrease in foam strut diameter. This decrease in diameter lowers the mechanical strength of the foam and increases the risk of micro-fracture within the foam matrix.

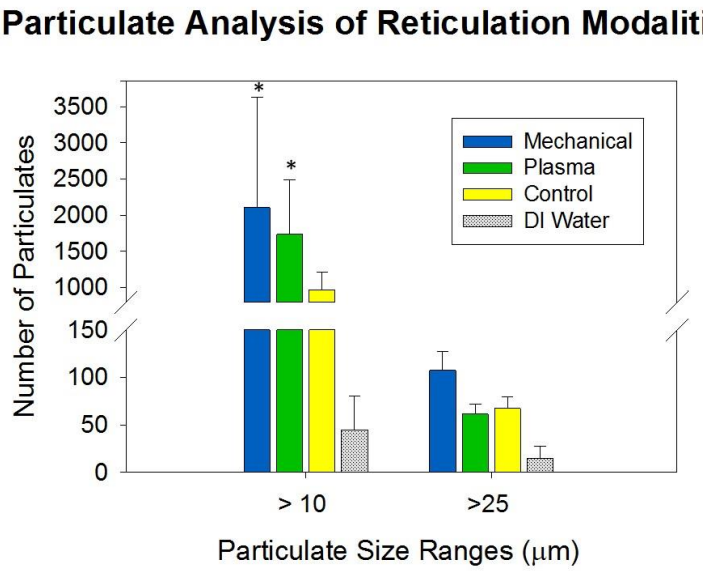

Figure 2.11: Particulates generated by mechanical and plasma reticulation. 100% TMHDI foam was used as a control and DI water particulate levels are recorded. n = 9; mean ± standard error displayed; *p < 0.05 relative to control.

2.4. Conclusions

The overarching goal of this study was to evaluate SMP foams as a candidate for a component of an NED on the basis of particulate generation. The results from this benchtop study indicate that particulates in the two ranges addressed by USP 788 (≥10 μm and ≥25 μm) are below the stated limits. While these limits do not directly address medical devices, they allow us to compare our materials to the most relevant standard. The third size range (≥50 μm) tested here does not have a limit defined by either the USP or FDA, but the level of particulates recorded in these experiments were very low for this size range. The results from the NR assay support the cytocompatibility of particulates generated from the SMP foams. Analysis of the reticulation modalities returned that plasma reticulation generates lower levels of particulates than mechanical reticulation. Furthermore, the cleaning protocol currently in place successfully lowers the particulate levels of the foams.

None of the three fillers resulted in particulate levels that would eliminate them as candidates for the device. The trends displayed in this study indicated that when varying weight and volume percentage W in the foams, a large increase (> 3%) in weight or volume percentage is required to produce significant increases in particulate levels.

Moving forward, there are some important considerations that need to be made. When selecting a foam composition for the neurovascular embolization device, it is important to consider that multiple foam devices are often deployed into the aneurysm sac during each procedure. Also, the volume of foam used in an embolization device will be substantially lower than the volume tested and must be evaluated separately on the basis of particulates. Further analysis will need to be performed to evaluate particulate generation after processing and during delivery on the benchtop.

CHAPTER III

QUANTIFICATION OF PARTICULATES GENERATED DURING DEVICE DELIVERY INTO BENCHTOP FLOW SYSTEMS

3.1 Introduction

After quantifying and characterizing the particulate levels of various SMP foams in Chapter II, the next step was to evaluate the device upon delivery into benchtop flow models that simulate a clinical embolization procedure. In a guidance document for a Class II medical device, the FDA recommends reporting the total quantity and size of particulates generated during simulated device use in three distinct size ranges ($\geq$10 μm, $\geq$25 μm, and $\geq$50 μm) to comprehensively report on any sub-visible particulate matter present[38].

The NED includes a pusher wire, attachment junction, and the foam-over-coil (FOC) implant. The assembly was subject to particulate analysis during acute application to remain in compliance with FDA recommendations[29]. Devices were delivered *via* microcatheter into a straight tube and a tortuous pathway model containing heated DI water. These experiments provided *in vitro* feedback on the amount of particulate matter that is generated during device delivery. The method and results for device fabrication, delivery, and particulate analysis are reported in this chapter.

3.2. Methods

3.2.1. Device fabrication

The device consists of SMP foam on a platinum wound nitinol backbone wire. HPED (99%), TEA (98%), TMHDI, and DI water are used to synthesize SMP foams using the three step method reported in Chapter II. Raw SMP foam is cleaned with a series of IPA and RO water sonications and tumbles, and then used in the assembly of neurovascular embolization

devices. The platinum wound nitinol wire was annealed over a mandrel in a furnace to give a helical shape, quenched in RO water, and cleaned using IPA and RO water[10]. SMP foam cylinders were cut using a 1 mm diameter biopsy punch. The nitinol wire was threaded axially through the SMP foam, and radially compressed using a heated stent crimper; the compressed SMP foam was secured to the nitinol wire using UV-cure epoxy (**Figure 3.1**)[10]. The completed device was laser welded to a guidewire to enable delivery *via* microcatheter during testing.

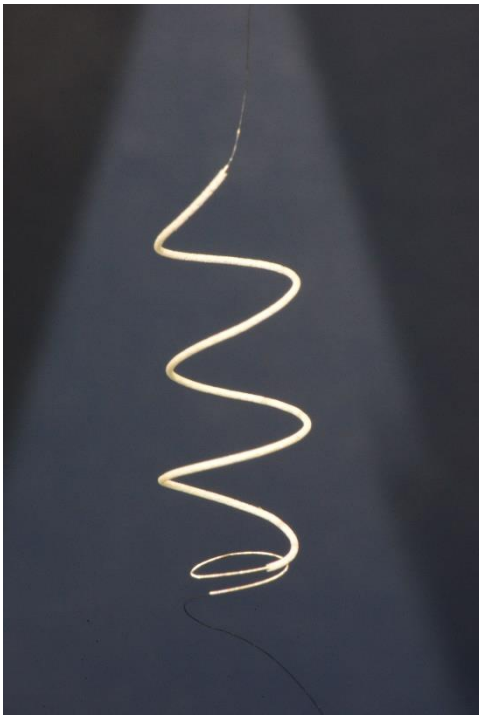

Figure 3.1: Fully assembled foam embolization device containing SMP foam crimped over platinum wound nitinol backbone wire. Helical diameter = 6 mm; foam length = 10 cm.

3.2.2. Delivery into a straight tube

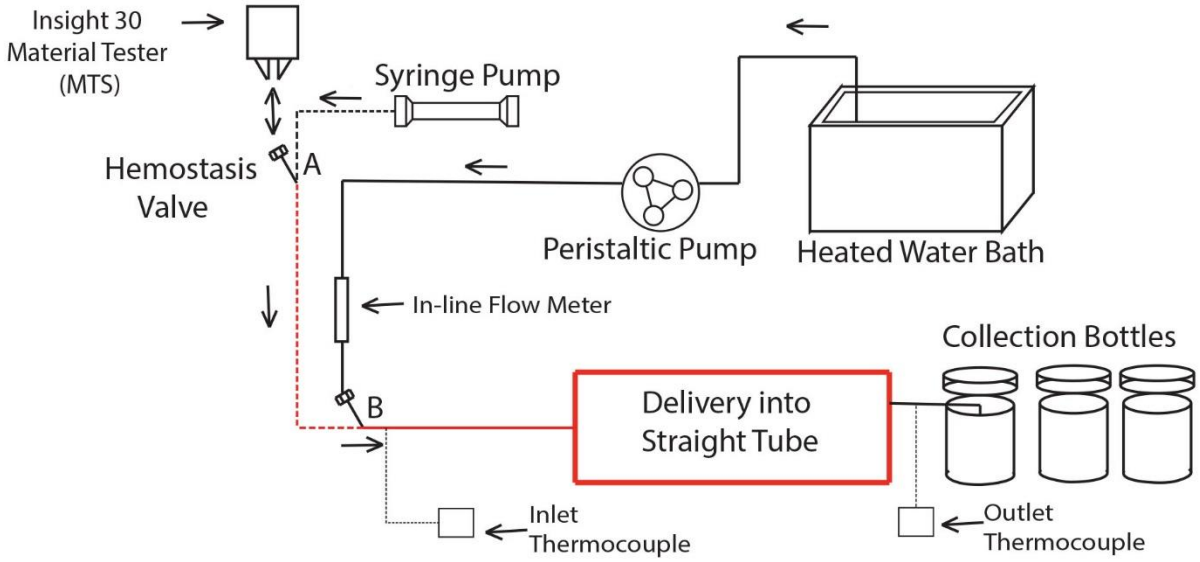

Figure 3.2: Schematic representation of the flow system to deliver devices into a straight tube. The red path denotes the microcatheter and the red box is the delivery zone. Device is inserted through hemostasis valve A.

Each experimental run consisted of delivery of one FOC implant *via* micro-catheter into a straight ¼" inner diameter tube (**Figure 3.2**) as DI water was pulled from a heated container *via* a peristaltic pump. The DI water was heated to an outlet temperature of 37° C, and pumps were adjusted to produce a flow rate of 100 ± 5 mL/min. A syringe pump was set to 0.4 mL/min to provide a constant flow of water within the microcatheter. Prior to device insertion, water from the flow system was collected from the outlet for 5 minutes to record the baseline particulate level of the flow system. Then, the device was inserted through hemostasis valve A (**Figure 3.2**) and manually advanced through the microcatheter until 1-3 mm of device was exposed at the distal tip of the microcatheter. Devices were cyclically advanced and retracted for 5 minutes using an Insight 30 Material Tester (MTS Systems Corporation, Eden Prairie, MN) or until stop criteria are observed. Stop criteria are denoted by (1) foam shearing,

(2) FOC to pusher detachment, (3) pusher buckling greater than 3 cm from the pushing plane, and/or (4) load exceeding 1.5 N absolute value (**Figure 3.3**). **Table 3.1** contains detailed descriptions for each stop criterion. Particulate collection began concurrently with device insertion through hemostasis valve A into the inner lumen of the microcatheter.

Table 3.1: Detailed descriptions of stop criteria for device delivery testing.

Stop Criteria	Description	Figure
Foam shearing	Foam delaminates from the coil, typically during retraction into the microcatheter, and fractures.	3.3A
FOC to pusher detachment	FOC stops moving with the pusher wire while pusher continues to push/pull through microcatheter	3.3B
Pusher buckling	Pusher buckles > 3 cm from the straight path at the proximal end out of the microcatheter without visible movement at the distal end	3.3C
Load exceeds 1.5 N	Real-time load measurement exceeds 1.5 N absolute value	---

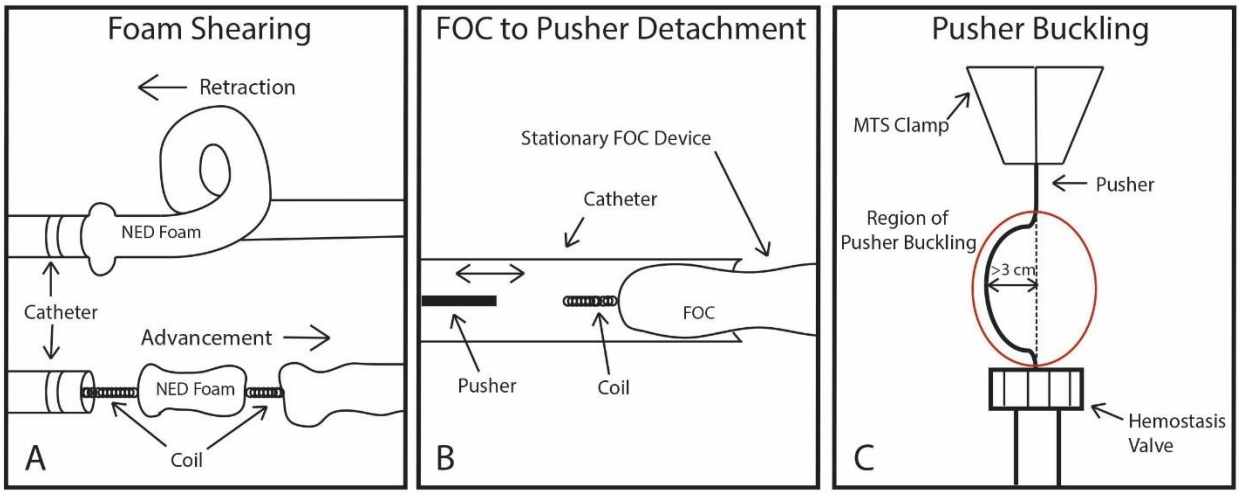

Figure 3.3: Stop criteria for the cyclic retraction testing of the embolization device. (A) Foam shearing, (B) FOC to pusher detachment, and (C) pusher buckling.

3.2.3. Delivery into a tortuous model

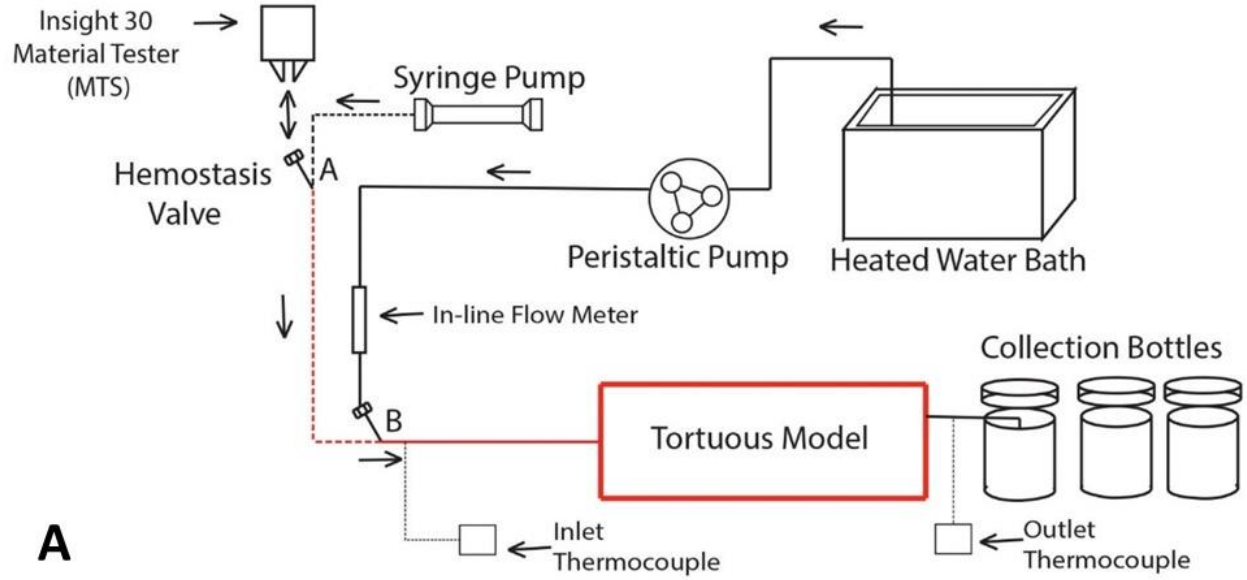

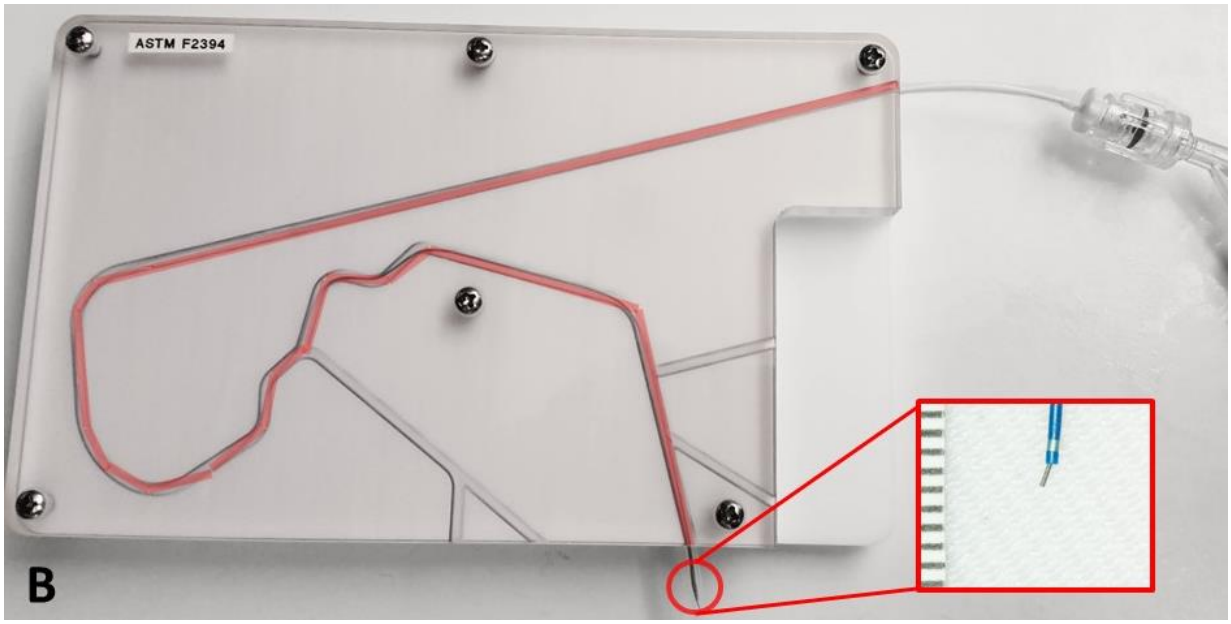

Figure 3.4: (A) Schematic representation of the flow system to deliver devices into a tortuous model. The red path denotes the microcatheter and the red box is the delivery zone. Device is inserted through hemostasis valve A. (B) Tortuous model used during testing. Microcatheter pathway is highlighted and a zoomed view of the device at the distal tip of the catheter is shown; scale is mm.

Each experimental run consisted of delivery of one FOC implant into a tortuous model *via* micro-catheter (**Figure 3.4B**) as DI water was pulled from a heated container *via* a peristaltic pump. The DI water was heated to an outlet temperature of 37° C, and pumps were adjusted to produce a flow rate of 31 ± 3 mL/min to simulate physiologic flow in a typical cranial artery[54]. A syringe pump was set to 0.4 mL/min to provide a constant flow of water within the microcatheter. Prior to device insertion, water from the flow system was collected from the outlet for 5 minutes to record the baseline particulate level of the flow system. Then, the device was inserted through hemostasis valve A (**Figure 3.4A**) and manually advanced through the microcatheter until 1-3 mm of device was exposed at the distal tip of the microcatheter (**Figure 3.4B**). Devices were cyclically advanced and retracted for 5 minutes using an Insight 30 Material Tester (MTS Systems Corporation, Eden Prairie, MN) or until stop criteria (**Figure 3.3 and Table 3.1**) were observed. Particulate collection began concurrently with device insertion through hemostasis valve A into the inner lumen of the microcatheter. One collection bottle was used for the entire 5-minute duration of the test.

3.2.4. Particulate analysis

In both the straight tube and tortuous model tests, each device produced two bottles containing particulate suspensions; one bottle contained the baseline particulates and the other contained the particulates generated during cyclic advancement and retraction of the device. The bottles were sonicated for one minute to re-suspend the particulates, and then analyzed using the particle counter.

3.3. Results and discussion

Device delivery into both a straight tube and tortuous model returned particulate levels that were below the thresholds stated in USP 788. The data was normalized by subtracting the

baseline particulate levels from the device levels. **Figure 3.5A** depicts the average particle levels recorded by the entire devices delivered into a straight tube. **Figure 3.5B** depicts the quantity of particulates per cm of device delivered. **Figure 3.6A and 3.6B** depict the average particulate levels for the device and per cm of device for embolization devices delivered into a tortuous model. In a clinical setting, the number of embolization devices that are implanted is dependent upon a number of different factors, including aneurysm size, FOC implant length, and physician satisfaction that the aneurysm is fully occluded[30].

Differences between the particulate levels in the straight tube delivery and the tortuous delivery are likely due to a number of inconsistencies between the two flow setups. Primarily, the length of tubing used in the tortuous path testing was substantially shorter than the straight tube testing causing the baseline particle levels to be lower in the tortuous flow model. Secondly, the flow rate used during straight tube delivery was approximately three times higher than the flow rate used in the tortuous testing. The change in flow rates was due to findings from a literature review that identified physiologic flow rates for vasculature in the cranial region where most clinical neurovascular embolization procedures are performed. In addition, the majority of device fabrication and benchtop testing for both tests was not performed in a clean room or laminar flow hood. Thus, the levels of environmental particulates present during processing and delivery were markedly higher than those expected from a final device that would be used in a clinical setting.

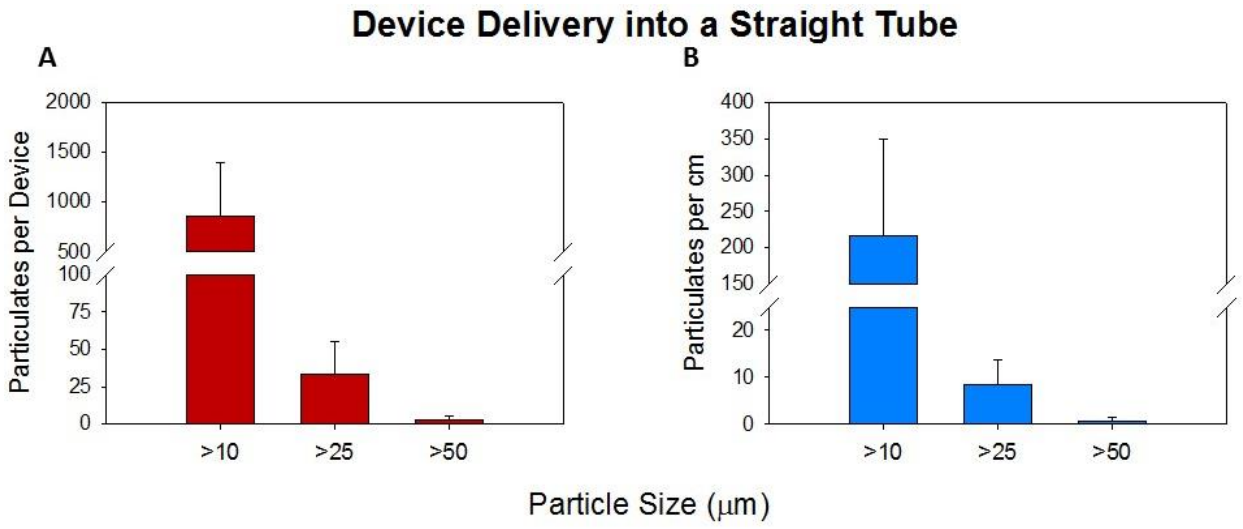

Figure 3.5: (A) Particulates recorded from delivery of a single embolization device into a straight tube in 3 size ranges. (B) Particulates per cm of device delivered in 3 different size ranges (n = 3).

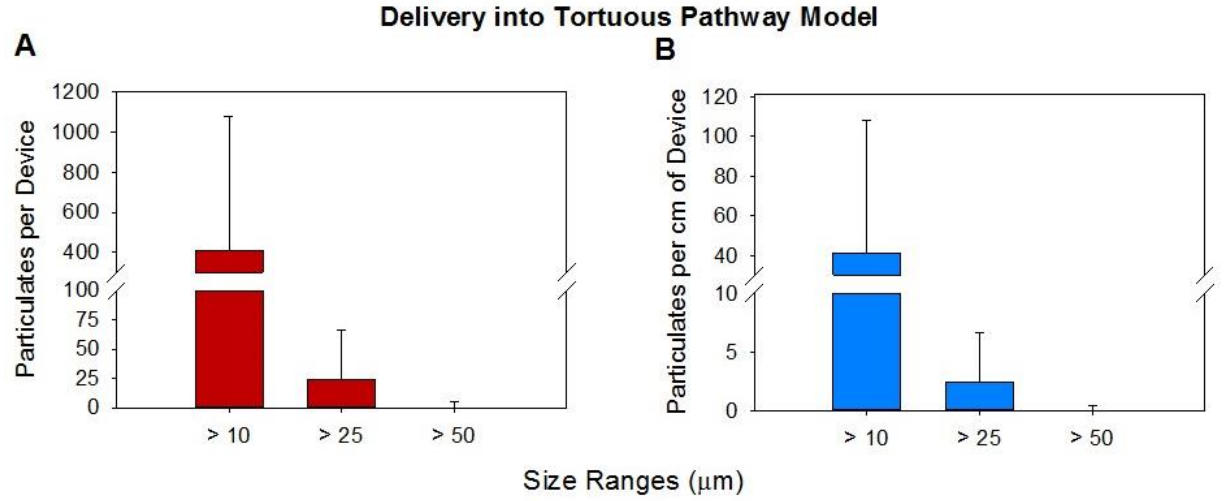

Figure 3.6: (A) Particulates recorded from delivery of a single embolization device into a tortuous pathway model in 3 size ranges. (B) Particulates per cm of device delivered in 3 different size ranges (n = 5).

3.4. Conclusions

Analysis of the embolization devices during delivery showed that the particulate levels are below the limits stated in the most relevant standard. Building on the results from Chapter II, this chapter further supports the use of SMP foam-based devices as promising candidates for embolization of cranial aneurysms. A definitive comparison between the straight tube testing and the tortuous pathway testing cannot be made because there was variability in test parameters such as flow rate and tubing length. The straight tube testing served as feasibility testing for the more rigorous tortuous pathway testing.

CHAPTER IV

CONCLUSIONS AND FUTURE WORK

4.1 Summary

SMP foams are promising candidates for endovascular occlusion applications because of their high volume recovery and ability to passively actuate at body temperature. The embolic risk posed by these devices is unknown and unreported. This thesis evaluated SMP foams and foam-based devices particulate generations. The FDA requires that particulate matter during processing, sterilization and delivery of medical devices be reported, but no prior work had been done to characterize particulate matter in these SMP foams. Initial protocols relied heavily on those outlined in USP 788, the standard for particulate matter in parenteral injections. The ability to quantify particulate levels enables mitigation of embolic risk posed by the foam-based embolization devices.

In Chapter II, bulk material analysis reflected that particle levels are in compliance with the particle limits defined in USP 788. Evaluation of the current cleaning protocol showed that it effectively reduces particulate levels. The particles and chemicals remaining within the foam matrix are driven out by the successive sonication and tumble cycles during cleaning. Thus, when analyzed post-cleaning, there are less loose foam struts and environmental particles within the foam that are generated by the agitation portion of the particulate quantification protocol. Reticulation of the foams was originally a cause for concern because it was hypothesized that the high friction involved in the mechanical reticulation process could generate unacceptable levels of particulates. This hypothesis was rejected upon particulate evaluation of the reticulation processes. While mechanical reticulation did produce the highest

particulate levels, they remained below the limits outlined in USP 788. Moving forward, neither plasma nor mechanical reticulation will drastically increase the levels of particulates generated by the foams. Overall, the best approach to mitigating particulate generation in bulk SMP materials is to minimize any mechanical forces that the foam is subject to in its glassy state ($< T_g$). Administering concentrated particulate treatments to fibroblasts showed that even a concentrated dose of particulates generated by a typical agitation cycle had a minimal effect on cell viability and supported the cytocompatibility of the SMP foams. In conclusion, bulk foams did not generate alarming levels of particulates.

Particulate analysis during device delivery built on the results from the bulk material testing by assessing the device in a clinically relevant benchtop flow system. Once inserted into the flow system, the device was cyclically maneuvered in and out of the microcatheter to simulate the worst-case scenario for device manipulation. Testing in worst-case scenarios helps to minimize performance related issues in the future. Testing returned that the devices generated particles at levels well below the USP standard. The results suggest that the device particle levels will remain below the USP limits even if multiple devices are implanted. This result is important, because clinical procedures typically involve the implantation of multiple embolic devices per aneurysm.

4.2 Challenges and future work

During the development of a protocol for quantifying particulates in SMP foams, LO was selected as the method of particle analysis using a suction based particle counter. Although the device is cost efficient and easy to use, there are several limitations. Specifically, suction fed devices require the user to leave a small exclusion volume that cannot be analyzed. While the excluded volume only accounts for a small percentage of the total sample volume, it may

alter the results. An alternative approach that addresses this issue is a gravity-fed particle counter. These devices allow for analysis of the entire sample volume so that results are representative of the whole sample. This method is desirable when working to quantify the whole sample volume.

In addition, further validation of the particle counter will be performed to ensure that the system is functioning as intended when recording larger particles. Validation will be performed by introducing a known quantity of particles 70 µm in diameter into the device and ensuring that at least 75% of the particles are recorded by the device. This will supplement the validation that was performed in Chapter III using 15 µm diameter microspheres. Upon purchase of the device, it was validated by the manufacturer, but providing in-house validation will be cost-effective and time efficient.

Similarly, the particle counter is limited in its ability to quantify particles larger than 200 µm. Larger particles pose a significantly higher risk of embolization. If introduced into blood circulation, a small number of these large particles could result in serious complications post-embolization. A future direction involves adding an additional step to the particulate quantification protocol. The particle suspension solution will first be filtered through a 200 µm filter, then the larger particles will be counted using a microscopy technique outlined in USP 788. Since the larger particles are visible under minimal magnification, quantification can be carried out in minimal time using a simple light microscope.

Upon evaluation of the flow setup for evaluating particulates generated during device delivery, some limitations were identified. First, the devices are delivered into a mock vessel with fluid continuously flowing past the device. In a clinical environment, the device is deployed into an aneurysm sac that is subject to reduced fluid velocities and differing flow

patterns. A future direction for delivery testing is to deliver the devices into a mock aneurysm model while flowing heated water past the aneurysm and collecting the water at the outlet for particulate analysis. This model will provide a more realistic simulation of flow parameters in the clinical procedure. Second, the tortuous model used does not simulate a worst-case scenario for cerebral tortuosity. A future direction involves increasing the tortuosity of the pathway that the microcatheter and device take to arrive at the delivery site. This method will provide a better idea of how the device will perform in difficult procedures, and limit future complications.

REFERENCES

[1] Lendlein, A., Kelch, S., *Shape-memory polymers.* Angewandte Chemie-Int, 2002. **41**: 2034 – 2057.

[2] Ratna, D., Karger-Kocsis, J., *Recent advances in shape memory polymers and composites: a review.* Journal Of Material Science, 2008. **43**: 254 – 269.

[3] DeNardo, L., Bertoldi, S., Tanzi, M.C., Haugen, H.J., Fare, S. *Shape memory polymer cellular solid design for medical applications.* Smart Materials and Structures, 2011. **20**: 1 – 13.

[4] Metcalfe, A., Desfaits, A.C., Salazkin, I., Yahia, L., Sokolowski, W., Raymond, J., *Cold hibernated elastic memory foams for endovascular interventions*. Biomaterials, 2003. **24**: 491 – 497.

[5] Hasan, S.M., Thompson, R.S., Emery, H., Nathan, A.L., Weems, A.C., Zhou, F., Wilson, T.S., Maitland, D.J., *Modification of Shape Memory Polymer Foams Using Tungsten, Aluminum Oxide, and Silicon Dioxide Nanoparticles*. Royal Society of Chemistry Advances, 2016. **6**: 918 – 927.

[6] Rodriguez, J., Yu, Y., Miller, M., Wilson, T., Hartman, J., Clubb, F., Maitland, D.J., *Opacification of Shape Memory Polymer Foam Designed for Treatment of Intracranial Aneurysms.* Annals of Biomedical Engineering, 2012. **40**(4): 883 – 897.

[7] Lendlein, A., Schmidt, A.M., Langer, R., *AB-polymer networks based on oligo(ε-caprolactone) segments showing shape-memory properties.* Proceedings of the National Academy of Sciences. **98**(3): 842 – 847.

[8] Hwang, W., Singhal, P., Miller, M.W., Maitland, D.J., *In vitro study of transcatheter delivery of a shape memory polymer foam embolic device for treating cerebral aneurysms*. Journal of Medical Devices, 2013. **7**: 20932 – 20933.

[9] Rodriguez, J.N., Clubb, F.J., Wilson, T.S., Miller, M.W., Fossum, T., Hartman, J., Tuzun, E., Singhal, P., Maitland, D.J., *In vivo response to an implanted shape memory polyurethane foam in a porcine aneurysm model*. Journal of Biomedical Materials Research Part A, 2013. **102**(5): 1231 – 1242.

[10] Boyle, A.J., Landsman, T.L., Wierzbicki, M.A., Nash, L.D., Hwang, W., Miller, M.W., Tuzun, E., Hasan, S.M., Maitland, D.J., *In vitro and in vivo evaluation of a shape memory polymer foam-over-wire embolization device delivered in saccular aneurysm models.* Journal of Biomedical Material Research Part B, 2015. Published online.

[11] Sokolowski, W., Metcalfe, A., Hayashi, S. Yahia, L., Raymond, J., *Medical applications of shape memory polymers.* Biomedical Materials, 2007. **2**: S23 – S27.

[12] Maitland, D.J., Small IV, W., Ortega, J.M., Buckley, P.R., Rodriguez, J., Hartman, J., Wilson, T.S., *Prototype laser-activated shape memory polymer foam device for embolic treatment of aneurysms*. Journal of Biomedical Optics, 2007. **12**(3): 1 – 3.

[13] Redekop, G., Willinsky, R., Montanera, W., TerBrugge, K., Tymianski, M., Wallace, M.C., *Endovascular occlusion of basilar bifurcation aneurysms with electrolytically detachable coils*. Canadian Journal of Neurological Science, 1999. **26**: 172 – 181.

[14] Singhal, P., Rodriguez, J.N., Small, W., Eagleston, S., Van de Water, J., Maitland, D.J., Wilson, T.S., *Ultra low density and highly crosslinked biocompatible shape memory polyurethane foams*. Journal of Polymer Science Part B: Polymer Physics, 2012. **50**(10): 724 – 737.

[15] Molyneux, A.J., Birks, J., Clarke, A., Sneade, M., Kerr, R.S.C., *The durability of endovascular coiling versus neurosurgical clipping of ruptured cerebral aneurysms: 18 year follow-up of the UK cohort of the International Subarachnoid Aneurysm Trial (ISAT).* Lancet, 2015. **385**: 691-698.

[16] Bederson, J.B., Connolly, E.S., Batjer, H.H., Dacey, R.G., Dion, J.E., Diringer, M.N., Duldner, J.E., Harbaugh, R.E., Patel, A.B., Rosenwasser, R.H., *Guidelines for the management of aneurysmal subarachnoid hemorrhage.* Stroke, 2009. **40**(3): 994 – 1025.

[17] Kumar, Abbas, and Aster. *Robbins and Cotran Pathologic Basis of Disease*. 9th Ed. 2014, Philadelphia, PA: Saunders/Elsevier.

[18] Hauser, S.C., Isselbacher, E.M., Zivin, J.A. *Goldman's Cecil Medicine.* 24th Ed. 2011, Philadelphia, PA: Saunders/Elsevier.

[19] Harada, K., Fukuyama, K., Shirouzu, T., Ichinose, M., Fujimura, H., Kakumoto, K., Yamanaga, Y., *Prevalence of unruptured intracranial aneurysms in healthy asymptomatic Japanese adults: differences in gender and age*. Acta Neurochirurgica, 2013. **155**: 2037 – 2043.

[20] Humphrey, J.D. *Cardiovascular Solid Mechanics: Cells, Tissues, and Organs.* 2002, New York: Springer.

[21] *Aneurysm Clipping.* [cited 2015 Nov 11], Available from: http://www.mayfieldclinic.com/PE-Clipping.htm

[22] Horowitz, M., Samsun, D., Purdy, P., *Does electrothrombosis occur immediately after embolization of an aneurysm with Guglielmi detachable coils?* American Journal of Neuroradiology, 1997. **18**: 510 – 513.

[23] *Endovascular Aneurysm Coiling.* [cited 2015 Nov 11], Available from: http://www.mayfieldclinic.com/PE-Coiling.htm#.Vk5FsXarTIU

[24] Murayama, Y., Nien, Y.L., Duckwiler, G., Gobin, Y.P., Jahan, R., Frazee, J., Martin, N., Viñuela, F., *Guglielmi detachable coil embolization of cerebral aneurysms: 11 years' experience.* Journal of Neurosurgery, 2003. **98**: 959 – 966.

[25] Guglielmi, G., Vinuela, F., Dion, J., Duckwiler, G., *Electrothrombosis of saccular aneurysms via endovascular approach, part 2: preliminary clinical experience*. Journal of Neurosurgery, 1991. **75**: 8 – 14.

[26] Suzuki, M., Yoneda, H., Ishihara, H., Shirao, S., Nomura, S., Koizumi, H., Suehiro, E., Goto, H., Sadahiro, H., Maruta, Y., Inoue, T., Oka, F., *Adverse events after unruptured cerebral aneurysm treatment: a single-center experience with clipping/coiling embolization combined units*. Journal of Stroke and Cerebrovascular Diseases, 2015. **24**: 223 – 231.

[27] Pandey, A.S., Koebbe, C., Rosenwasser, R.H., Veznedaroglu, E., *Endovascular coil embolization of ruptured and unruptured posterior circulation aneurysms: Review of a 10-year experience.* Neurosurgery, 2007. **60**(4): 626 – 634.

[28] Szikora, I., Seifert, P., Hanzely, Z., Kulcsar, Z., Berentei, Z., Marosfoi, M., Czirjak, S., Vajda, J., Nyary, I., *Histopathologic evaluation of aneurysms treated with Guglielmi detachable coils or Matrix detachable microcoils.* American Journal of Neuroradiology, 2006. **27**: 283 – 288.

[29] Ortega, J., Maitland, D.J., Wilson, T.S., Tsai, W. Savas, O., Saloner, D., *Vascular dynamics of a shape memory polymer foam aneurysm treatment technique.* Annals of Biomedical Engineering, 2007. **35**(11): 1870 – 1884.

[30] Kallmes, D.F., Fujiwara, N.H., Yuen, D., Dai, D., Li, S., *A collagen-based coil for embolization of saccular aneurysms in a New Zealand white rabbit model.* American Journal of Neuroradiology, 2003. **24**: 591 – 596.

[31] Gunnarsson, T., Klurfan, P. terBrugge, K.G. Willinsky, R.A., *Treatment of intracranial aneurysms with hydrogel coated expandable coils.* Canadian Journal of Neurological Science, 2007. **34**: 38 – 46.

[32] Raymond, J., Guilbert, F. Weill, A., Geroganos, S., Juravsky, L., Lambert, A., Lamoureux, J., Chagnon, M., Roy, D., *Long-term angiographic recurrences after*

selective endovascular treatment of aneurysms with detachable coils. Stroke, 2003. **34**: 1398 – 1403.

[33] Cloft, H.J., Kallmes, D.F., *Aneurysm packing with hydrocoil embolic system versus platinum coils: initial clinical experience.* American Journal of Neuroradiology, 2004. **25**: 60 – 62.

[34] Poncyljusz, W., Zarzycki, A., Zwarzany, L., Burke, T.H., *Bare platinum coils vs. HydroCoil in the treatment of unruptured intracranial aneurysms – A single center randomized controlled study.* European Journal of Radiology, 2015. **84**: 261 – 265.

[35] Geyik, S., Yavuz, K., Cekirge, S., *Endovascular treatment of basilar and ICA termination aneurysms: effects of the use of HydroCoils on treatment stability in a subgroup of patients prone to a higher recurrence rate.* Neuroradiology, 2007. **49**: 1015 – 1021.

[36] McDougall, C.G., Claiborne Johnston, S., Gholkar, A., Barnwell, S.L., Vazquez Suarez, J.C., Masso Romero, J., Chaloupka, J.C., Bonafe, A., Wakhloo, A.K., Tampieri, D., Dowd,, C.F., Fox, A.J., Imm, S.J., Carroll, K., *Bioactive versus bare platinum coils in the treatment of intracranial aneurysms: The MAPS (Matrix and Platinum Science) Trial.* American Journal of Neuroradiology, 2014. **35**: 935 – 942.

[37] United States Pharmacopeia (USP) 788: Particulate Matter in Injections. The United States Pharmacopeial Convention 2011.

[38] FDA CDRH Class II Special Controls Guidance Document for Certain Percutaneous Transluminal Coronary Angioplasty (PTCA) Catheters, guidance document 1608, 2010.

[39] AAMI TIR42: 2010, *Evaluation of particulates associated with vascular medical devices* (Arlington, VA: AAMI, 2010).

[40] FDA Guidance on Non-Clinical Engineering Tests and Recommended Labeling for Intravascular Stents and Associated Delivery Systems [cited 2015 January 10]. Available from: http://www.fda.gov/medicaldevices/deviceregulationandguidance/guidancedocuments/ucm071863.htm

[41] Cui, J., Chen, S., Zhang, C., Meng, F., Wu, W., Hu, R., Hadass, O., Lehmidi, T., Blair, G.J., Lee, M., Chang, M., Mobashery, S., Sun, G.Y., Gu, Z., *Inhibition of MMP-9 by a selective gelatinase inhibitor protects neurovasculature from embolic focal cerebral ischemia*. Molecular Neurodegeneration, 2012. 7 – 21.

[42] Gwinn, M.R., Vallyathan, V., *Nanoparticles: Health Effects: Pros and Cons*. Environmental Health Perspectives, 2006. **114**(12): 1818 – 1825.

[43] Lim, Y., Turco, S., Davis, N.M., *Particulate matter in small-volume parenterals as determined by two methods.* Journal of Hospital Pharmacology, 1973. **30**: 518 – 525.

[44] PC5000 Operations Manual: Basic Theory of Operation. *Chemtrac Inc*. Norcross, GA 2014.

[45] Hergenrother, R., *Evolution of coatings for endovascular devices*. Rubber World, 2013. 27 – 29.

[46] Hasan, S.M., Raymond, J.E., Wilson, T.S., Keller, B.K., and Maitland, D.J., *Effects of Isophorone Diisocyanate on the Thermal and Mechanical Properties of Shape-Memory Polyurethane Foams*. Macromolecular Chemistry and Physics, 2014. **215**: 2420 – 2429.

[47] Hasan, S.M., Harmon, G., Zhou, F., Raymond, J.E., Gustafson, T.P., Wilson, T.S., Maitland, D.J., *Tungsten-loaded SMP foam nanocomposites with inherent radiopacity and tunable thermal-mechanical properties*. Polymer Advanced Technologies 2015.

[48] Rodriguez, J.N., Miller, M.W., Boyle, A., Horn, J., Yang, C., Wilson, T.S., Ortega, J.M., Small, W., Nash, L., Skoog, H., Maitland, D.J., *Reticulation of low density shape memory polymer foam with an in vivo demonstration of vascular occlusion.* Journal of the Mechanical Behavior of Biomedical Materials, 2014. **40**: 102 – 114.

[49] Blair, E.A., *Cell Structure: Physical property relationships in elastomeric foams.* National Academy of Sciences, National Research Council, 1966. Natick, MA 143 – 152.

[50] Rivera, N. *Characterization of cold plasma reticulated shape memory polymer foam.* Master's Thesis, 2015, Texas A&M University, State College, TX.

[51] Repetto, G., Peso, A., Zurita, J.L., *Neutral red uptake assay for the estimation of cell viability/cytotoxicity*. National Institute of Toxicology and Forensic Sciences, 2008. **3**(7): 1125 – 1132.

[52] Laurent, A. *Microspheres and nonspherical particles for embolization.* Techniques in Vascular and Interventional Radiology, 2007. **10**: 248 – 256.

[53] Cieslicki, K., Ciesla, D., *Investigations of flow and pressure distributions in physical model of the circle of Willis.* Journal of Biomechanics, 2005. **38**: 2302 – 2310.

APPENDIX

Validation and verification of LO particle counter

Validation and verification are important processes that confirm that a system is performing as intended. Validation shows, through objective evidence, that a system will perform as intended. Similarly, verification shows, through objective evidence, that system requirements have been fulfilled. Validation of the LO particle counter was performed by introducing a known quantity of particles of a known size into the device and ensuring that at least 75% are recovered. The accuracy of the particle counter used throughout these studies was verified using an alternative method for particulate quantification.

Method

Microscopy evaluation is provided in USP 788 as an alternate approach to LO when quantifying particles in solution. The same inversion protocol as outlined in Chapter II, Section 2.5 was followed to generate particles from the sample. Then, the sample solution was filtered through a 10 µm – pore filter assembly and examined with a binocular microscope. The filter was placed over a 5 cm x 5 cm grid and manually counted on a binocular light microscope (Leica MZ 16, Meyer Instruments, Houston, TX). LO counts were performed to compare against the microscopy counts. 100% TMHDI foams synthesized using the steps outlined in Chapter II, Section 2.2. Phloxine, a red dye making the foam bright pink, was incorporated during synthesis to maximize visibility under the microscope.

Results and discussion

Particulate analysis using both LO and microscopy on foams with identical compositions returned that the microscopy technique performed was unable to detect particles ranging from

10 – 25 µm. **Figure A-1A** displays particle levels in the phloxine foams in three size ranges. **Figure A-1B** displays only one size range for the microscopy technique because only one filter (10 µm pores) was used in the assembly. This result shows that the particle levels recorded by the microscopy technique are correspondent with counts for particles ≥25 µm for the LO particle counter. There are a number of reasons why this could have happened. First, the microscope resolution was limited to approximately 25 µm, making it very difficult to discern small particles (10 – 25 µm). Second, particle aggregates were difficult to quantify under microscope. Lastly, microscopy counts were performed by counting the number of particles trapped in the 10 µm – pore filter. This approach made it difficult to see any smaller particles trapped in the body of the filter (filter thickness = 300 µm). In comparison, LO is a faster, more repeatable process with higher resolution. Validation of the LO particle counter, however, is a necessary step to ensure that the device is functioning as specified in the requirements.

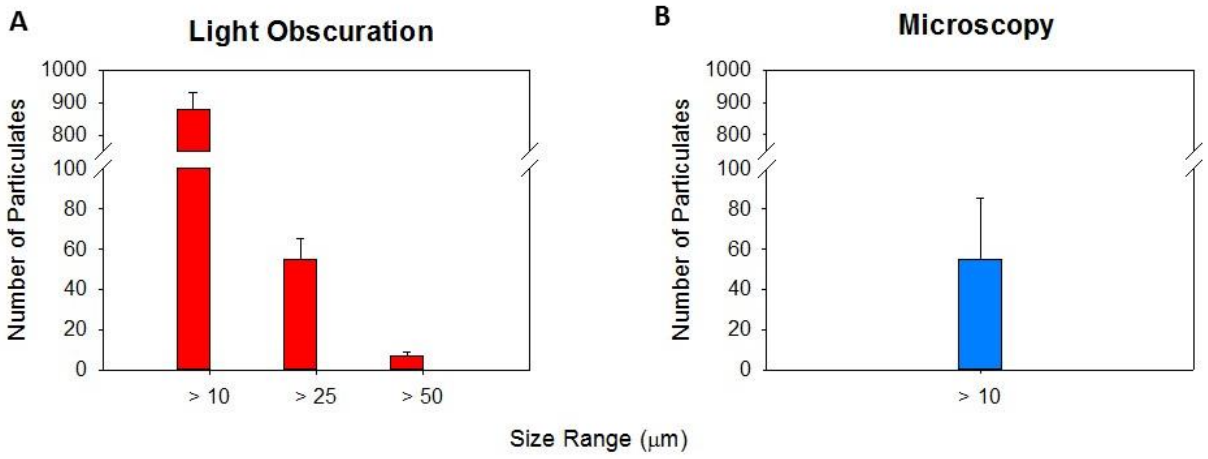

Figure A-1: Two particle quantification techniques: (A) LO and (B) microscopy; n = 3.